Mixed Control Moment Gyro and Momentum Wheel Attitude Control Strategies

C. Eugene Skelton II

Thesis submitted to the Faculty of the
Virginia Polytechnic Institute and State University
in partial fulfillment of the requirements for the degree of

Master of Science
in
Aerospace Engineering

Dr. Christopher Hall, Committee Chair
Dr. Fred Lutze, Committee Member
Dr. Craig Woolsey, Committee Member

November 21, 2003
Blacksburg, Virginia

Keywords: Mixed Control Strategies, Control Moment Gyro, Momentum Wheel,
Spacecraft Simulator, Attitude Control

Abstract

Mixed Control Moment Gyro and Momentum Wheel Attitude Control Strategies

C. Eugene Skelton II

Attitude control laws that use control moment gyros (CMGs) and momentum wheels are derived with nonlinear techniques. The control laws command the CMGs to provide rapid angular acceleration and the momentum wheels to reject tracking and initial condition errors. Numerical simulations of derived control laws are compared. A trend analysis is performed to examine the benefits of the derived controllers. We describe the design of a CMG built using commercial off-the-shelf (COTS) equipment. A mixed attitude control strategy is implemented on the spacecraft simulator at Virginia Tech.

Acknowledgments

I would like to thank my advisor, Dr. Chris Hall, for his support and patience while I was coming up the learning curve of spacecraft dynamics and control. Dr. Hall offered excellent individual instruction, and should be commended for organizing an ideal environment for cooperative learning in the lab.

Honeywell Aerospace deserves thanks for funding my research of mixed actuator attitude control. It was their financial support that facilitated the design, construction, and implementation of a CMG on the spacecraft simulator.

Special thanks goes to the graduate and undergraduate students of the Space Systems Simulation Laboratory that helped machine, assemble, wire, code, and debug the spacecraft simulator, Whorl-I. I would not have simulator results without their assistance. They are (in reverse alphabetical order): Matt VanDyke, Andrew Turner, Bret Streetman, Mike Shoemaker, Jana Schwartz, Marcus Pressl, Scott Lennox, and Cengiz Akinli.

Contents

List of Figures

List of Tables

Chapter 1

Introduction

1.1 Background

Spacecraft cover a broad range of missions with differing system requirements. Spacecraft range in size from picosats to space stations. Some spacecraft have autonomous control, while others have no dynamic control. Spacecraft maneuverability is dependent on mission requirements.

A common example of a spacecraft with an interesting mission is the Hubble Space Telescope, which must maneuver to and hold an orientation in inertial space. Hubble uses four reaction wheels and magnetic torquers for attitude control [1]. The time for reorientations is on the order of tens of minutes, an acceptable period for Hubble's mission.

Certainly different missions dictate the acceptable period for a maneuver. A spacecraft designed to intercept objects coming into the atmosphere might require the ability to slew one half of a revolution in seconds and then track an object which is moving at a high velocity. Such large slew, high-rate maneuvers can be achieved with differing types of actuators, and possibly combinations of actuators. Strategies for maneuvers can be adapted for attitude maintenance, that are needed because of aerodynamic, gravity gradient, and solar wind perturbations.

Common actuators for applying torques are thrusters and magnetic torquers. Thrusters provide torque on the spacecraft by expelling propellant. Magnetic torquers use the earth's magnetic field to generate torque on the spacecraft. There are limitations to both thrusters and magnetic torquers.

Thrusters require propellant, which must be launched with the spacecraft at consider-

able cost. The exhausted propellant can affect sensitive equipment such as optics. The changing mass of the spacecraft, movement of the center of mass, and changing inertia tensor, make control laws more complex. Attitude maintenance using thrusters requires low impulse capability. Low thrust diminishes the rapid slewing ability of a spacecraft.

Advantages of magnetic torquers are that they have no moving components and they do have replenishment power supply with solar power. However they typically provide small torque which is not acceptable for rapid slewing. The magnetic field of the earth or any primary body varies in strength and direction depending on orbital position, which adds complexity to control derivation and modelling.

Other means of applying torque to a spacecraft involve momentum exchange devices such as momentum wheels and control moment gyros. Momentum exchange devices work through the conservation of angular momentum. Conservation of angular momentum states that the angular momentum of a system without external torques is constant in the inertial frame. From conservation of angular momentum we know that a body and flywheel system has an angular momentum equal to the sum of its individual momenta, and it is constant in the inertial frame for all time provided there are no external torques. Changing the flywheel's angular momentum will affect the body's angular momentum and *vice versa*. There are two common devices for angular momentum exchange, momentum wheels and control moment gyros.

A momentum wheel consists of a flywheel that spins about a fixed axis in the body. The flywheel is generally axisymmetric and spins about its axis of symmetry. Angular momentum is exchanged between the flywheel spin axis and the body by applying a torque with a motor. The acceleration of the body about the spin axis of the momentum wheel is related to the change in angular momentum of the momentum wheel and the inertia of the body about the momentum wheel spin axis. Typically there are four momentum wheels mounted in such a way that there is redundancy for three-axis control. The maximum acceleration of the body from the momentum wheel is limited by the maximum torque of the motor.

The control moment gyro (CMG) is a momentum exchange device that can produce large output torque on the body. A CMG has a flywheel that spins at a constant velocity relative to the CMG frame. The spin axis of the flywheel can vary about a perpendicular axis to its spin axis. We call this perpendicular axis the gimbal axis. Complex dynamic derivations are used to find a relationship between the torque input to gimbal axis and a desired output torque on the body. The rate of change of angular momentum between the CMG and the body is dependent on the gimbal velocity. An unwanted result of varying the spin axis of the flywheel is that there can be orientations where no output

torque can be given in a certain direction; these orientations result in singularities in the control laws. Typically singularities are avoided by either using a pyramid of four CMGs or by deriving a controller that is "smart enough" to avoid singular orientations. Concepts that use other actuators with CMGs or variable-speed CMGs have also been explored for singularity avoidance.

The concept of mixed actuator attitude control attempts to take advantage of the strong aspects of certain devices while using other devices to compensate for the weaknesses of the first set devices. An example is the use of thrusters and momentum wheels [2], where the thruster provide coarse rapid acceleration and the momentum wheels provide fine tuning of attitude and angular velocity. Certainly there is the advantage of redundancy with multiple attitude control actuators; however the price of redundancy is hardware, launch cost, and control complexity.

The general problem that we address is spacecraft reorientation and high-speed tracking. More generally the problem is determining the current attitude and angular velocity of a body, determining a desired attitude and angular velocity, and determining the control inputs to the devices that will drive the current attitude and angular velocity to the desired. The means of solving for the inputs can be simple or complex depending on the devices and initial error between the current and desired states. The control laws that determine the inputs to the devices have been the subject of many studies.

Another way of thinking about the problem is to determine the path in state space to get from the current to the desired attitude and angular velocity. The complexity of path determination is dependent on the devices and the initial error. For any rotation an Euler axis and Euler angle can be found to be the most direct path between the initial and desired attitude. The minimum time reorientation is achieved by accelerating at maximum torque about the Euler axis to half of the Euler angle, and then decelerating at maximum torque to the desired attitude if the Euler axis is aligned with a principle axis. The minimum time reorientation uses "bang-bang" control. In real spacecraft the ability to apply maximum torque about any Euler axis is generally not possible. Moreover, the off-diagonal terms of the inertia for a spacecraft will cause off-Euler axis rotations about the Euler axis if the Euler axis does not coincide with a principal axis.

Common means of validating control laws are numerical simulation and implementation on a physical apparatus that reflects attributes of the real system to be controlled. Numerical simulations are effective at demonstrating control concepts in an ideal environment at minimal cost. For this research numerical simulations of a rigid body with three CMGs and three momentum wheels are performed without the hardware cost of each device. Spacecraft simulators are apparatuses for physical implementation that gen-

erally consist of a body with varying rotational and translational freedom. Simulators can vary from single degree of rotational or translational freedom to full six degree of freedom systems [3].

The purpose of this research is to explore the use of control moment gyros for rapid coarse slewing maneuvers and momentum wheels for fine tuning of attitude and angular velocity. The momentum wheels can adjust for initial condition errors, and tracking errors. The effectiveness of derived control laws is measured by control effort, accuracy, and time required for a maneuver. Numerical simulation and implementation on a spacecraft simulator validate the derived control laws and strategies. *

1.2 Research Overview

The goal of this research is to develop control laws that use control moment gyros for large reorientations or rapid tracking and momentum wheels for error rejection. Ford [4] developed the equations of motion for a rigid body with gimballed momentum wheels. Ford's equations are modified to represent a rigid body with CMGs and momentum wheels. Equations of motion of a virtual reference body are developed. A body fixed reference frame in the virtual reference body defines the desired motion for tracking.

Control laws are developed that use angular velocity and attitude feedback for tracking of a reference trajectory. Modified Rodrigues Parameters (MRPs) are used to describe the attitude of the body and virtual reference frame. A Lyapunov control law introduced in Ref. [5] and modified in Ref. [2] is expanded to account for the control moment gyros' dynamics. A control strategy provides open loop actuation of the CMGs with closed loop control from the momentum wheels, where the feedback control law may or may not have knowledge of the CMG's maneuvering. Various closed loop control laws that use both CMGs and momentum wheels are developed.

A mathematical model of a rigid body with CMGs and momentum wheels is developed to evaluate the effectiveness of control laws. The model has full rotational freedom. Numerical simulation of the control laws are performed.

The control laws derived are tested on the Distributed Spacecraft Attitude Control Systems Simulator in the Space Systems Simulation Lab at Virginia Tech. A CMG was designed, fabricated, assembled, tested, and integrated into the simulator with use of commercial off-the-shelf (COTS) components. Large slew maneuvers are performed on the simulator to illustrate the control strategy.

*http://www.aoe.vt.edu/research/groups/sssl/

1.3 Outline of Thesis

A review of the literature is presented in Chapter 2. Specific attention is given to studies that use CMGs or momentum wheels for attitude control of spacecraft. Work directed toward reorientations and mixed control strategies is presented. An overview of other spacecraft simulators is presented.

In Chapter 3 we cover the kinematics and equations of motion for a rigid body with CMGs and momentum wheels. The attitude representation is Modified Rodrigues Parameters. The equations of motion are expressed in vector form. The control inputs are momentum wheel spin axis torques and CMG gimbal axis torques.

Spacecraft reorientations and tracking are addressed in Chapter 4. Error functions for attitude and angular velocity are defined. Lyapunov control laws are derived for reference body tracking. A feedback linearization control law is developed for use with the momentum wheels as error rejection. Other strategies that use CMGs and momentum wheels together in feedback are presented, along with a CMG feedback and momentum wheel feedforward control law. Several variations of the developed control laws are presented.

For each derived controller numerical simulation results are presented. The results are shown in Chapter 5. A trend analysis of varying reorientation rates for selected control laws is shown. A control effort quantification for the simulated control laws is presented. Maximum control torques for differing reorientation rates and controllers are examined.

The control moment gyro designed, built, and tested from COTS equipment is reviewed in Chapter 6. Reviews of the sizing of the CMG's flywheel and actuators are shown. The structure is briefly discussed. Chapter 6 also specifically reviews the Distributed Spacecraft Attitude Control System Simulator (DSACSS). Hardware limitations and spacecraft simulator rotational freedom constraints prevent the derived controllers from direct implementation on DSACSS. A control law presented in Section 4.5.5 is simplified to include a single CMG and three orthogonal momentum wheels for testing on DSACSS. Simulator results are presented in Chapter 6.

A summary of the research and conclusions of the results are presented in Chapter 7.

Chapter 2

Literature Review

In this chapter we present an overview of investigations that use momentum exchange devices for attitude control. There have been many studies that effectively use momentum wheels or CMGs for attitude control. Discussion of singularity avoidance is often included with CMG attitude control studies. Mixed actuator attitude control strategy studies are investigated. Spacecraft simulators are briefly covered with a reference to a thorough review of spacecraft simulators.

2.1 Momentum Exchange Devices

Momentum exchange devices include momentum wheels and control moment gyros. Any general body that contains a rotating axisymmetric body is called a *gyrostat*. The axisymmetric body is a *momentum wheel*. Hughes [6] provided a complete derivation of the dynamic equations for a gyrostat. Hall [7] extended Hughes's derivation to include multiple momentum wheels. Several studies have used momentum wheels for multiple tasks, such as using momentum wheels for energy storage and attitude control [8, 9, 10]. Junkins *et al.* [11] used nonlinear adaptive control with three orthogonal momentum wheels to provide near optimal reorientations of spacecraft. They proposed that open loop commands could be derived while solving the inverse dynamics of the system. Modified Rodrigues Parameters were used for attitude representation.

The equations of motion are presented in a Newton-Euler derivation in Ref. [12] for a rigid body with N CMGs. Feedback control laws using gimbal rates and gimbal accelerations are formulated using Lyapunov theory. Specific attention was given to the gimbal rate steering law presented in order to take advantage of the "torque amplification" factor

of the CMGs. Vadali *et al.* [13] showed that singularities can be avoided with certain choices of the initial gimbal angles for a known maneuver. Vadali *et al.* [14, 15] presented new methods for generation of open-loop and closed-loop CMG commands based on Lyapunov control theory that used Euler angle and angular velocity errors as the states for the controller.

Ford [4] derived a new form of the equations of motion for a rigid body with gimballed momentum wheels that used a Newton-Euler approach. The equations contained the gimbal axis and spin axis torques explicitly for the gimballed momentum wheels. Ford showed that adding special restrictions to the equations of motion would result in the equations of motion for a rigid body with either momentum wheels or control moment gyros. Euler-Bernoulli appendages were added to the system equations using a Lagrangian approach. Reorientation control laws with singularity avoidance were presented with attention put toward not exciting the flexible appendages.

In Ref. [16] Ford and Hall used the equations developed in Ref. [4] for a rigid body with single gimbal control moment gyros to modify the *Singularity Robust Steering Law* of Ref. [12]. The modification used singular value decomposition to compute the pseudo inverse in order to steer the CMGs away from singular configurations. Ford and Hall proved that the torque error from singularity avoidance was always less with *Singular Direction Avoidance* than with *Singularity-Robust Steering Law* [4, 16].

Rokui and Kalaycioglu [17] performed an input-output feedback linearization on the dynamics of a rigid body that used CMG gimbal accelerations. The system equations were formed with Euler angles and angular momenta. A linear PID controller was implemented in the linearized system for attitude control. The gimbal acceleration control law was proven to cause the system to converge asymptotically; however the control law produced undesirable jitter in the system.

The equations of motion and energy equations for a rigid body with variable speed control moment gyros (VSCMGs) were derived by Schaub *et al.* in Ref. [18]. The primary difference between Ref. [4] and Ref. [18] is that the equations did not specify the gimbal motor torque explicitly as Ford did. The Lyapunov function presented by Tsiotras in Ref. [5] is used to develop control laws for a rigid body with VSCMGs in Ref. [18]. Both gimbal velocity and gimbal acceleration control laws are developed, with some attention to singularity avoidance using the VSCMG with null motion for CMG reorientation. The work of Ref. [18] was mainly an extension of Ref. [12].

Avanzini and de Metteis [19] adapted the CMG feedback control law of Ref. [12] into a feedforward steering law. The concept was based on inverse simulation of the dynamics to find the required gimbal angles and rates from a desired attitude. Gimbal torques

were computed for open loop commands.

Heiberg *et al.* [20] showed that a Variable Periodic Disturbance Rejection Filter (VPDRF) with CMG actuation suppressed non-linear disturbances. The disturbances originated from small gimbal displacements or "CMG ripple" which was fed back through the control loop resulting in a cascading disturbance. The VRDRF effectively rejected internal and external disturbances.

In Ref. [21] Heiberg *et al.* focused on rapid reorientation for multiple-target acquisition with CMG feedback control. A nonlinear control law was based on quaternion error feedback, with consideration to actuator constraints such as saturation and bandwidth limit.

Singh and Bossart [22] presented an exact feedback linearization of the roll, pitch, and yaw rates for the Space Station with gravity torques that used CMGs. The resulting closed loop system was linearly controllable; however the system was unstable for large reorientations. The feedback linearization control law was suitable for slow maneuvers like that of Space Station. The control law was not suitable for large rapid reorientations because of kinematic singularities.

Research that used momentum exchange devices to control spacecraft attitude and tracking has been discussed. The referenced works used angular velocity and attitude for states of their control laws. Different attitude representations in feedback control laws are discussed in the next section.

2.2 Effects of Attitude Representation on Lyapunov Control

The chosen attitude representation is related to the performance of controllers. Singularities and nonlinearities from certain attitude representations negatively affect the control performance. Nonlinear control laws can perform linearly with certain attitude representations, such as MRPs [5].

Various studies have used Lyapunov control laws with quaternions, Euler Angles, and Modified Rodrigues Parameters for attitude feedback. Tsiotras [5] presented a Lyapunov function that utilized the three-parameter set of Modified Rodrigues Parameters (MRPs) for attitude feedback. The Lyapunov function led to linear feedback controllers that globally asymptotically stabilize the attitude. Many studies have since used this Lyapunov function for attitude control using momentum exchange devices.

Long [23] used Tsiotras's MRPs Lyapunov function to derive momentum wheel actuated control laws for spacecraft target tracking. The target that Long choose for reference tracking was the sun vector.

Casasco and Radice [24] developed Lyapunov control laws that used either quaternion or MRP feedback. A new linearized MRPs representation was introduced and used in a Lyapunov control law effectively for small reorientations. Pointing constraint avoidance was added to the derived controllers.

2.3 Mixed Control Strategies

Recently more attention has been directed toward using combinations of actuators for attitude control. The concept of mixed actuator attitude control attempts to take advantage of the strengths of each individual type of actuator. The advantage of mixed actuator control is that the undesirable characteristics of a type of actuator can be avoided while taking advantage of their strengths. For example, Hall *et al.* [2] showed that using thrusters to provide large torques for reorientation and momentum wheels for fine tuning of attitude utilized the strengths of both actuators. The small torques required for attitude tuning are not ideally produced by thrusters because of their discontinuous nature; however momentum wheels are well suited for this role. In the same way momentum wheels are not ideal for producing large output torques because the output torque is directly related to the torque applied by the motor to the flywheel. Thrusters are better suited for larger coarse output torques. Chen and Steyn [25] utilized the same logic of Hall *et al.* [2, 9] to derive a mixed thruster and momentum wheel attitude control law. The momentum wheels were driven by both open and closed loop quaternion and angular velocity error control laws.

Roithmayr *et al.* [26] derived the equations of motion for a spacecraft with single gimbal control moment gyros and flywheels with Kane's method. The gimbal frames of the CMGs were assumed massless, unlike Ford's derivation. Large reorientations were considered to be the burden of both types of actuators. The concept was that the control torque required would be halved so that each type of actuator would act independently with their sum meeting the overall torque requirements. We wish to take advantage of the strengths of each actuator rather than simply distributing the burden.

The mixed combination of magnetic torquers and CMGs for attitude control was explored by Lappas *et al.* [27]. The magnetic torquers were used for external disturbance rejection and gimbal angle maintenance in order to avoid singularities and control constraints. Oh and Vadali's [12] CMG gimbal rate steering law was used for attitude control. The benefit

of this configuration was that momentum dumping was addressed without additional hardware. However, the attitude reorientation benefits from the ability to optimally align the gimbal angles were marginal. Schaub and Junkins [28] used a similar approach to configure optimally the gimbal angles of the CMG cluster. With null motion steering laws derived for Variable Speed Control Moment Gyros or Gimballed Momentum Wheels the gimbal angles can be rearranged away from singular configurations for improved CMG feedback control performance.

Mixed actuator control laws have shown advantages over homogenous actuator control laws in previous research. Numerical simulations were generally used to validate the controllers. Spacecraft simulators were another method used to validate the derived controllers.

2.4 Spacecraft Simulators

A spacecraft simulator is a device that can imitate the rotational or translational freedom of a real spacecraft. Implementation of control actuators on spacecraft simulators for validation of control strategies has been performed since the beginning of the space program [3]. Momentum exchange devices are readily used on spacecraft simulators since they do not rely on the Space environment like thrusters and magnetic torques. Honeywell Aerospace has developed an air bearing test bed which uses a pyramid configuration of single gimbal control moment gyros for attitude control algorithm testing [29]. References [30, 31] integrated double gimballed momentum wheels into an air bearing spacecraft simulator for control validation. Reference [32] presents a constrained steering law for a pyramid configuration of CMGs and the implementation on a spacecraft simulator test bed. The simulator was a hanging structure mounted to a three-axis gimbal. The derived control laws were demonstrated effectively on the simulator.

Spacecraft simulator systems have been developed at the Air Force Institute of Technology [33], the University of Michigan [34], and the Georgia Institute of Technology [35]. A comprehensive look at spacecraft simulators from the beginning of the space program to the present is presented by Schwartz *et al.* [3]. A description of the Distributed Spacecraft Attitude Control System Simulator being developed at Virginia Tech is included in the article.

The works described in this chapter laid the ground work for this research. We now consider the equations of motion for a spacecraft that uses CMGs and momentum wheels for attitude actuation. Modified Rodrigues Parameters are used for attitude representation.

Chapter 3

Kinematics and Dynamics

Here we present the equations that describe a rigid body with CMGs and momentum wheels. We use Modified Rodrigues Parameters (MRPs) to describe the kinematics. The equations that describe the system and control axis momenta are derived from Euler's rotational equations by Ford [4]. Ford's equations are modified to describe a rigid body with N CMGs and M momentum wheels.

3.1 Kinematics

There are many common methods to describe the attitude reorientations such as Euler Angles, Euler Axis/Angles, Euler Parameters (Quaternions), and Modified Rodrigues Parameters. Euler's Theorem states that any rotation about a single fixed point can be described by a rotation about a fixed axis through that point. The axis and angle are generally called the Euler axis and Euler angle, respectively. It is common to denote $\hat{\mathbf{e}}$ as the Euler axis and Φ as the Euler angle. For this research we choose to use MRPs because singularities can be avoided with use of the shadow set. Also, with careful selection of a Lyapunov function we can derive linear controllers with use of MRP identities [5].

3.1.1 Modified Rodrigues Parameters

The three element set of MRPs is defined as

$$\boldsymbol{\sigma} = \hat{\mathbf{e}} \tan(\Phi/4) \tag{3.1}$$

Singularities occur when $\Phi = 360n$ where n is an integer. Singularities are avoided with use a shadow set of MRPs [36]

$$\boldsymbol{\sigma}^S = -\frac{1}{\boldsymbol{\sigma}^T\boldsymbol{\sigma}}\boldsymbol{\sigma} \tag{3.2}$$

The shadow set replaces the original MRPs when $\boldsymbol{\sigma}^T\boldsymbol{\sigma} > 1$ to avoid singularities. The magnitude of the MRP that switches to the shadow set is user defined. The conversion from MRPs to a direction cosine matrix is

$$\mathbf{R} = \mathbf{1} + \frac{4(1-\boldsymbol{\sigma}^T\boldsymbol{\sigma})}{(1+\boldsymbol{\sigma}^T\boldsymbol{\sigma})^2}\boldsymbol{\sigma}^\times + \frac{8}{(1+\boldsymbol{\sigma}^T\boldsymbol{\sigma})^2}(\boldsymbol{\sigma}^\times)^2 \tag{3.3}$$

With knowledge of the angular velocity between two reference frames we can describe the rotation between the two reference frames by integrating

$$\dot{\boldsymbol{\sigma}} = \mathbf{G}(\boldsymbol{\sigma})\boldsymbol{\omega} \tag{3.4}$$

where $\boldsymbol{\omega}$ is the relative angular velocity of one frame with respect to the other frame and

$$\mathbf{G}(\boldsymbol{\sigma}) = \frac{1}{2}\left(\mathbf{1} + \boldsymbol{\sigma}^\times + \boldsymbol{\sigma}^T\boldsymbol{\sigma} - \frac{1+\boldsymbol{\sigma}^T\boldsymbol{\sigma}}{2}\mathbf{1}\right) \tag{3.5}$$

We have defined the kinematics as a function of the angular velocity. The equations of motion allow us to find the angular velocity of the spacecraft. In the next section we derive the equations of motion for a rigid body with N CMGs and M momentum wheels.

3.2 Dynamics

This section presents the derivation of the angular momentum of the system. The angular momenta of the actuator control axes (gimbal axes for the CMGs and spin axes for the momentum wheels) are developed. A Newton-Euler approach is taken to derive the momenta. An equation for all of the gimbal angles of the CMGs is shown. A summary of the equations of motion concludes this section. We start with the definition of the system and inertias.

3.2.1 System Definition

Consider a rigid body with N control moment gyros (CMGs), and M momentum wheels. The body is generally asymmetric. A body-fixed reference frame, $\mathcal{F}_b$, has unit axes

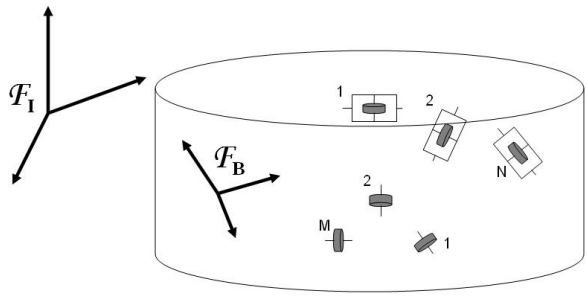

Figure 3.1: *System with CMGs and Momentum Wheels*

defined by $(\vec{\mathbf{b}}_1, \vec{\mathbf{b}}_2, \vec{\mathbf{b}}_3)$(see Figure 3.1). The body is free to rotate in the inertial reference frame, $\mathcal{F}_I$. Each CMG has a reference frame, $\mathcal{F}_{G_j}(j = 1...N)$, with unit axes $(\vec{\mathbf{a}}_{sj}, \vec{\mathbf{a}}_{tj}, \vec{\mathbf{a}}_{gj})$ denoted spin, transverse, and gimbal axes, respectively (see Figure 3.2). The origin of $\mathcal{F}_{G_j}$ is at the center of mass of the j-th CMG. The vector components of $(\vec{\mathbf{a}}_{sj}, \vec{\mathbf{a}}_{tj}, \vec{\mathbf{a}}_{gj})$ are assumed to be given in $\mathcal{F}_b$. The unit vector $\vec{\mathbf{a}}_{gj}$ is in the direction of the CMG gimbal axis and fixed in $\mathcal{F}_b$. The flywheel rotates at a constant relative velocity about the spin axis which is orthogonal to the gimbal axis. The transverse axis is orthogonal to the gimbal and spin axes. We denote the gimbal angle of the j-th CMG as δ_j. Given some initial gimbal angle, δ_{j0}, the spin and transverse axes are

$$\vec{\mathbf{a}}_{sj}(t) = \cos(\delta_j(t) - \delta_{j0})\vec{\mathbf{a}}_{sj}(0) - \sin(\delta_j(t) - \delta_{j0})\vec{\mathbf{a}}_{tj}(0) \tag{3.6}$$

$$\vec{\mathbf{a}}_{tj}(t) = \sin(\delta_j(t) - \delta_{j0})\vec{\mathbf{a}}_{sj}(0) + \cos(\delta_j(t) - \delta_{j0})\vec{\mathbf{a}}_{tj}(0) \tag{3.7}$$

Using this notion we define a $3\times N$ matrix, $\mathbf{A}_s$, whose columns are $\vec{\mathbf{a}}_{sj}$ such that

$$\mathbf{A}_s = [\vec{\mathbf{a}}_{s1}, \vec{\mathbf{a}}_{s2}, ..., \vec{\mathbf{a}}_{sN}] \tag{3.8}$$

Matrices $\mathbf{A}_t$ and $\mathbf{A}_g$ are defined in the same manner. The gimbal orientation matrix $\mathbf{A}_g$ is constant, while $\mathbf{A}_s$ and $\mathbf{A}_t$ vary with gimbal angles. The relative angular velocity of the j-th flywheel to its gimbal frame is $\Omega_j\vec{\mathbf{a}}_{sj}$. An $N \times 1$ matrix $\mathbf{\Omega}$ is formed as $[\Omega_1, \Omega_2, ..., \Omega_N]^T$. The angular velocity of $\mathcal{F}_{G_j}$ relative to $\mathcal{F}_b$ is $\dot{\delta}_j\vec{\mathbf{a}}_{gj}$. A matrix $\dot{\boldsymbol{\delta}}$ is formed as $[\dot{\delta}_1, \dot{\delta}_2, ..., \dot{\delta}_N]^T$.

The momentum wheels are defined in a similar manner as the CMGs. Each momentum wheel has a reference frame $\mathcal{F}_{W_k}(k = 1...M)$ whose 3 axis aligns with the spin axis. The spin axis and thus the 3 axis of $\mathcal{F}_{W_k}$ is fixed in the body. The vector components of the unit axes $(\vec{\mathbf{c}}_{sk}, \vec{\mathbf{c}}_{tk}, \vec{\mathbf{c}}_{gk})$ are assumed to be given in $\mathcal{F}_b$. We define a matrix

$$\mathbf{C}_s = [\vec{\mathbf{c}}_{s1}, \vec{\mathbf{c}}_{s2}, ..., \vec{\mathbf{c}}_{sM}] \tag{3.9}$$

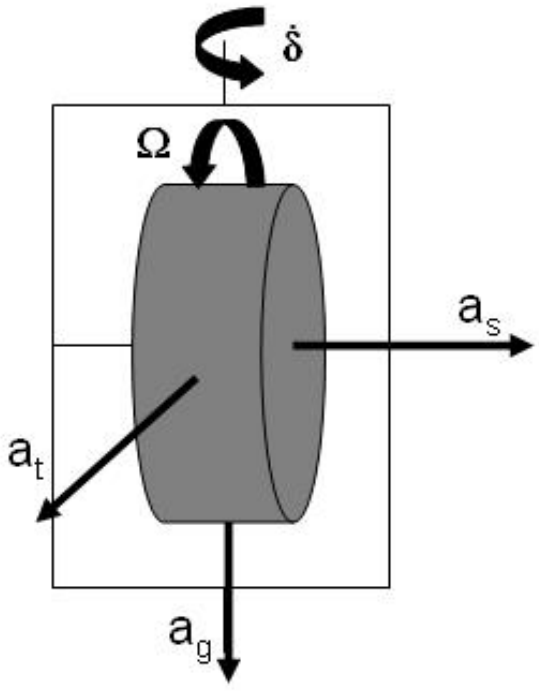

Figure 3.2: *Control Moment Gyro*

to describe the spin axes of the momentum wheels. The relative angular velocity of the k-th flywheel is $\Omega_{MWk}\vec{\mathbf{c}}_{sj}$. A matrix $\mathbf{\Omega}_{MW}$ is formed as $[\Omega_{MW1}, \Omega_{MW2}, ..., \Omega_{MWM}]^T$.

3.2.2 Moment of Inertia

The mass of the body is assumed constant. The moment of inertia for the entire system is assumed constant except for changes caused by the varying CMG gimbal angles. The center of mass of the CMGs is assumed to be fixed in the body. Thus the center of mass of the system is constant in the body. An inertia-like tensor formed from the body, momentum wheels, and the parallel axis contributions from the CMGs is

$$\vec{I}_B = \vec{I}_P + \sum_{k=1}^{M} m_k(\vec{\mathbf{r}}_k \cdot \vec{\mathbf{r}}_k\vec{1}... - \vec{\mathbf{r}}_k\vec{\mathbf{r}}_k) + \sum_{j=1}^{N} m_j(\vec{\mathbf{r}}_j \cdot \vec{\mathbf{r}}_j\vec{1}... - \vec{\mathbf{r}}_j\vec{\mathbf{r}}_j) \tag{3.10}$$

The first term on the right hand side is the inertia tensor of the principal body. The transverse inertias for the momentum wheels are included in the principal body inertia. We define m_j and m_k as the mass of the j-th CMG and k-th momentum wheel, respec-

tively. The vector from the center of mass of the system to the center of mass of the j-th CMG is $\vec{\mathbf{r}}_j$. The vector from the center of mass of the system to the center of mass of the k-th momentum wheel is $\vec{\mathbf{r}}_k$.

The inertia of the j-th CMG in $\mathcal{F}_{Gj}$ can be expressed as $\text{diag}(I_{sj}, I_{tj}, I_{gj})$ where I_{sj}, I_{tj}, I_{gj} represent the spin axis inertia, transverse inertia, and gimbal axis inertia. Note that the frame inertias are included. We wish to separate the inertia of the flywheel from the inertia of the frame in the spin axis. We set $I_{sj} = I_{swj} + I_{sgj}$ where I_{swj} is the inertia of the flywheel and I_{sgj} is the inertia of the CMG frame and motor about the spin axis. We form a matrix

$$\mathbf{I}_{sw} = \text{diag}(I_{sw1}, I_{sw2}, ..., I_{swN}) \tag{3.11}$$

along with three more matrices $\mathbf{I}_{sg}$, $\mathbf{I}_t$, and $\mathbf{I}_g$ which are formed in the same manner. We form an additional matrix like the CMG flywheel inertia matrix for the momentum wheels, $\mathbf{I}_{swMW} = \text{diag}(I_{swMW1}, I_{swMW2}, ..., I_{swMWM})$. We represent the total inertia of the system in $\mathcal{F}_B$ as

$$\mathbf{I} = \mathbf{I}_B + \mathbf{A}_s(\mathbf{I}_{sw} + \mathbf{I}_{sg})\mathbf{A}_s^T + \mathbf{A}_t\mathbf{I}_t\mathbf{A}_t^T + \mathbf{A}_g\mathbf{I}_g\mathbf{A}_g^T + \mathbf{C}_s\mathbf{I}_{swMW}\mathbf{C}_s^T \tag{3.12}$$

where $\mathbf{I}_B$ represents the tensor from Equation 3.10 in the body-fixed reference frame.

The inertias of the body, and the actuators have been defined. We use the inertias to find the angular momentum of the system.

3.2.3 Angular Momentum

We assume that the center of mass of the system is an inertial origin. The angular momentum of the body about its center of mass is

$$\vec{\mathbf{h}} = \vec{\mathbf{I}}_P \cdot \vec{\boldsymbol{\omega}} + \sum_{j=1}^{N} \vec{\mathbf{h}}_{CMGja} + \sum_{k=1}^{M} \vec{\mathbf{h}}_{MWka} \tag{3.13}$$

where $\vec{\mathbf{h}}_{CMGja}$ and $\vec{\mathbf{h}}_{MWka}$ are the absolute angular momenta of the j-th CMG and the k-th MW about their own center of mass, respectively. The absolute angular velocity of $\mathcal{F}_\mathcal{B}$ is $\vec{\boldsymbol{\omega}}$. The inertia of the whole system is $\vec{\mathbf{I}}$. The absolute angular momentum of the j-th CMG is defined by

$$\vec{\mathbf{h}}_{CMGja} = \vec{\mathbf{I}}_j \cdot \vec{\boldsymbol{\omega}}^{G_j i} \tag{3.14}$$

where $\vec{\mathbf{I}}_j$ is the inertia tensor of the j-th CMG. The absolute angular velocity of $\mathcal{F}_{G_j}$ is $\vec{\boldsymbol{\omega}}^{G_j i}$. Recall the assumption that the center of mass of the CMG is constant in $\mathcal{F}_B$. Expressed in the body-fixed frame the absolute angular momentum of the j-th CMG is

$$\mathbf{h}_{CMGja} = \mathbf{I}_j(\boldsymbol{\omega}^{bi} + \boldsymbol{\omega}^{G_j b}) \tag{3.15}$$

To simplify notation $\boldsymbol{\omega}$ will be the angular velocity of $\mathcal{F}_b$ with respect to $\mathcal{F}_i$. We separate the absolute angular momentum into components in the spin, transverse, and gimbal directions

$$\begin{aligned} h_{sja} &= I_{sj}\mathbf{a}_{sj}^T\boldsymbol{\omega} + I_{sj}\Omega_j && (3.16)\\ h_{gja} &= I_{gj}\mathbf{a}_{gj}^T\boldsymbol{\omega} + I_{gj}\dot{\delta}_j && (3.17)\\ h_{tja} &= I_{tj}\mathbf{a}_{tj}^T\boldsymbol{\omega} && (3.18) \end{aligned}$$

The absolute angular momentum of the spin axis of the j-th CMG is split into

$$h_{sja} = h_{swja} + h_{sgja} \tag{3.19}$$

where h_{swa} represents the absolute angular momentum of the flywheel about the spin axis, and h_{sga} the absolute angular momentum of the gimbal frame and motor about the spin axis.

The absolute angular momentum of the k-th MW is defined as

$$\vec{\mathbf{h}}_{kMWa} = \vec{\mathbf{I}}_k \cdot \vec{\boldsymbol{\omega}}^{W_k i} \tag{3.20}$$

where $\vec{\boldsymbol{\omega}}^{W_k i}$ is the absolute angular velocity of the momentum wheel. The spin axis angular momentum of the k-th MW is an $M \times 1$ matrix $\mathbf{h}_{swMWka}$.

The angular momentum of the system in the body-fixed frame is

$$\mathbf{h} = \mathbf{I}_B\boldsymbol{\omega} + \mathbf{A}_s\mathbf{h}_{sa} + \mathbf{A}_t\mathbf{h}_{ta} + \mathbf{A}_g\mathbf{h}_{ga} + \mathbf{C}_s\mathbf{h}_{sMWa} \tag{3.21}$$

where we define $\mathbf{h}_{sa} = [h_{s1a}, ..., h_{sNa}]^T$. We define $\mathbf{h}_{ta}$, $\mathbf{h}_{ga}$, and $\mathbf{h}_{sMWa}$ in the same manner.

We write the absolute angular momentum of the actuators as the sum of the angular momentum due to the body's angular velocity and the actuator's relative angular velocity.

$$\begin{aligned} \mathbf{h}_{swa} &= \mathbf{I}_{sw}\mathbf{A}_s^T\boldsymbol{\omega} + \mathbf{h}_{swr} && (3.22)\\ \mathbf{h}_{sga} &= \mathbf{I}_{sg}\mathbf{A}_s^T\boldsymbol{\omega} + \mathbf{h}_{sgr} && (3.23)\\ \mathbf{h}_{ta} &= \mathbf{I}_t\mathbf{A}_t^T\boldsymbol{\omega} + \mathbf{h}_{tr} && (3.24)\\ \mathbf{h}_{ga} &= \mathbf{I}_g\mathbf{A}_g^T\boldsymbol{\omega} + \mathbf{h}_{gr} && (3.25)\\ \mathbf{h}_{swMWa} &= \mathbf{I}_{swMW}\mathbf{C}_s^T\boldsymbol{\omega} + \mathbf{h}_{swMWr} && (3.26) \end{aligned}$$

Notice that the CMGs are constrained to 2 degrees of freedom with respect to the body, gimbal angle and flywheel spin, therefore

$$\mathbf{h}_{sgr} = \mathbf{h}_{tr} = 0 \tag{3.27}$$

The total angular momentum simplifies to

$$\mathbf{h} = (\mathbf{I}_B + \mathbf{A}_t\mathbf{I}_t\mathbf{A}_t^T + \mathbf{A}_s\mathbf{I}_{sg}\mathbf{A}_s^T)\boldsymbol{\omega} + \mathbf{A}_s\mathbf{h}_{swa} + \mathbf{A}_g\mathbf{h}_{ga} + \mathbf{C}_s\mathbf{h}_{swMWa} \tag{3.28}$$

The end goal is to determine equations that govern the angular momentum of the body along with the angular momenta of the components of each CMG and momentum wheel. An equation for the gimbal angle is also developed. From dynamics we know that the absolute time derivative of any vector $\vec{\mathbf{x}}$ in the inertial frame can be defined by the time derivative of $\vec{\mathbf{x}}$ in some frame $\mathcal{F}_P$ plus the angular velocity of $\mathcal{F}_P$ with respect to the inertial frame crossed with the vector $\vec{\mathbf{x}}$. That is,

$$\left[\frac{d\vec{\mathbf{x}}}{dt}\right]_i = \left[\frac{d\vec{\mathbf{x}}}{dt}\right]_P + \vec{\boldsymbol{\omega}} \times \vec{\mathbf{x}} \tag{3.29}$$

The absolute time derivative of angular momentum in the inertial frame is

$$\dot{\vec{\mathbf{h}}} = \vec{\mathbf{v}} \times \vec{\mathbf{p}} + \vec{\mathbf{g}}_e \tag{3.30}$$

where $\vec{\mathbf{v}}$ and $\vec{\mathbf{p}}$ are the linear velocity and momentum, respectively. The external torques on the system are $\vec{\mathbf{g}}_e$. Recall the assumption that the center of mass of the system is translationally fixed in inertial space, therefore $\vec{\mathbf{p}} = \mathbf{0}$. The change in angular momentum can be expressed in $\mathcal{F}_b$ as

$$\dot{\mathbf{h}} = -\boldsymbol{\omega}^{\times}\mathbf{h} + \mathbf{g}_e \tag{3.31}$$

where the superscript $\times$ refers to the skew symmetric matrix of the vector such as

$$\boldsymbol{\omega}^{\times} = \begin{bmatrix} 0 & -\omega_3 & \omega_2 \\ \omega_3 & 0 & -\omega_1 \\ -\omega_2 & \omega_1 & 0 \end{bmatrix} \tag{3.32}$$

We have defined the the angular momentum of the system. We now develop the equations to describe the actuators. The torque inputs to the actuators are the control inputs for the system. We start with the CMG gimbal angles.

3.2.4 Gimbal Angles

To develop the gimbal angles we start by substituting

$$h_{gr} = I_{gj}\mathbf{a}_g^T\boldsymbol{\omega}^{G_j b} = I_{gj}\dot{\delta}_j \tag{3.33}$$

into the absolute angular momentum of the CMG about the gimbal axis Equation 3.25. From the absolute gimbal angular momentum we have an integrable equation for gimbal angle that is

$$\dot{\delta}_j = I_{gj}^{-1} h_{gja} - \mathbf{a}_g^T \boldsymbol{\omega} \tag{3.34}$$

A general way to write all N integrable equations for gimbal angles is

$$\dot{\boldsymbol{\delta}} = \mathbf{I}_g^{-1} \mathbf{h}_{ga} - \mathbf{A}_g^T \boldsymbol{\omega} \tag{3.35}$$

With an equation for gimbal angle defined we form matrices $\boldsymbol{\Delta}^c$ and $\boldsymbol{\Delta}^s$ where

$$\boldsymbol{\Delta}^c = \text{diag}(\cos \boldsymbol{\delta}) \tag{3.36}$$

$$\boldsymbol{\Delta}^s = \text{diag}(\sin \boldsymbol{\delta}) \tag{3.37}$$

where $\cos \boldsymbol{\delta}$ and $\sin \boldsymbol{\delta}$ are the cosine and sine of the of each term in $\boldsymbol{\delta}$. The initial gimbal matrices are defined as $\mathbf{A}_{s0}$ and $\mathbf{A}_{t0}$. These matrices represent $\mathbf{A}_s$ and $\mathbf{A}_t$ when the gimbal angles are at δ_{j0}. As a function of gimbal angle $\mathbf{A}_s$ and $\mathbf{A}_t$ are

$$\mathbf{A}_s = \mathbf{A}_{s0} \boldsymbol{\Delta}^c + \mathbf{A}_{t0} \boldsymbol{\Delta}^s \tag{3.38}$$

$$\mathbf{A}_t = -\mathbf{A}_{s0} \boldsymbol{\Delta}^s + \mathbf{A}_{t0} \boldsymbol{\Delta}^c \tag{3.39}$$

The time rate of change of $\mathbf{A}_s$ and $\mathbf{A}_t$ is

$$\dot{\mathbf{A}}_s = \mathbf{A}_t \text{diag}(\dot{\boldsymbol{\delta}}) \tag{3.40}$$

$$\dot{\mathbf{A}}_t = -\mathbf{A}_s \text{diag}(\dot{\boldsymbol{\delta}}) \tag{3.41}$$

The gimbal angles for all N CMGs have been defined. The CMG control input changes the gimbal angle. We develop the gimbal momenta to define the control input to the CMG.

3.2.5 Gimbal Momenta

We want to develop an equation that describes the gimbal angular momentum of the j-th CMG. The gimbal axis is the control axis for the CMGs. The gimbal axis torque is

$$g_{gj} = \vec{\mathbf{a}}_{gj} \cdot \vec{\mathbf{g}}_{CMGj} \tag{3.42}$$

where $\vec{\mathbf{g}}_{CMGj}$ is the torque that the body exerts on the j-th CMG. We see that the absolute angular momentum of the j-th CMG about the gimbal axis is

$$h_{gja} = \vec{\mathbf{a}}_{gj} \cdot \vec{\mathbf{h}}_{CMGj} \tag{3.43}$$

The time derivative of h_{gja} is

$$\dot{h}_{gja} = \dot{\vec{\mathbf{a}}}_{gj} \cdot \vec{\mathbf{h}}_{CMGj} + g_{gj} \tag{3.44}$$

where the time derivative of the unit vector $\vec{\mathbf{a}}_{gj}$ is

$$\dot{\vec{\mathbf{a}}}_{gj} = \vec{\boldsymbol{\omega}} \times \vec{\mathbf{a}}_{gj} \tag{3.45}$$

Using the vector identity $(\vec{\mathbf{a}} \times \vec{\mathbf{b}}) \cdot \vec{\mathbf{c}} = \vec{\mathbf{a}} \cdot (\vec{\mathbf{b}} \times \vec{\mathbf{c}})$, equation 3.44 can be rewritten as

$$\dot{h}_{gja} = \vec{\boldsymbol{\omega}} \cdot (\vec{\mathbf{a}}_{gj} \times \vec{\mathbf{h}}_{CMGj}) + g_{gj} \tag{3.46}$$

We separate the gimbal and wheel angular momenta

$$\vec{\mathbf{h}}_{CMGj} = \vec{\mathbf{I}}_{gj} \cdot \vec{\boldsymbol{\omega}}^{G_j i} + \vec{\mathbf{I}}_{wj} \cdot (\vec{\boldsymbol{\omega}}^{G_j i} + [\Omega_j, 0, 0]^T) \tag{3.47}$$

where

$$\vec{\boldsymbol{\omega}}^{G_j i} = \dot{\boldsymbol{\delta}}_j \vec{\mathbf{a}}_{gj} + \vec{\boldsymbol{\omega}} \tag{3.48}$$

$$\vec{\mathbf{I}}_{wj} = I_{tj} \vec{\mathbf{1}} + (I_{sj} - I_{tj}) \vec{\mathbf{a}}_{sj} \vec{\mathbf{a}}_{sj} \tag{3.49}$$

Substituting into equation 3.46 leads to

$$\dot{h}_{gja} = \vec{\boldsymbol{\omega}} \cdot (\vec{\mathbf{a}}_{gj} \times (\vec{\mathbf{I}}_{wj} \cdot (\Omega_j \vec{\mathbf{a}}_{sj} + \dot{\delta}_j \vec{\mathbf{a}}_{gj} + \vec{\boldsymbol{\omega}}) + \vec{\mathbf{I}}_g \cdot (\dot{\boldsymbol{\delta}} \vec{\mathbf{a}}_g + \vec{\boldsymbol{\omega}}))) + \mathbf{g}_{gj} \tag{3.50}$$

which we can integrate to find the absolute angular momentum of the gimbal axis of the j-th CMG.

To expand this equation for all gimbal angular momenta we write

$$\dot{\mathbf{h}}_{ga} = \vec{\boldsymbol{\omega}} \cdot (\vec{\mathbf{A}}_g \times (\boldsymbol{\Omega} \vec{\mathbf{A}}_s + \dot{\boldsymbol{\delta}} \vec{\mathbf{A}}_g + \vec{\boldsymbol{\omega}}) + \vec{\mathbf{I}}_g \cdot (\dot{\boldsymbol{\delta}} \vec{\mathbf{A}}_g + \vec{\boldsymbol{\omega}})) + \mathbf{g}_g \tag{3.51}$$

This equation can be simplified as shown in Ref. [4] to

$$\dot{\mathbf{h}}_{ga} = \mathrm{diag}((\mathbf{I}_t - \mathbf{I}_{sg}) \mathbf{A}_s^T \boldsymbol{\omega} - \mathbf{h}_{swa})(\mathbf{A}_t^T \boldsymbol{\omega}) + \mathbf{g}_g \tag{3.52}$$

The equation for the CMGs gimbal axis angular momentum provides a useful means of implementing control by keeping the gimbal axis torque term separate.

3.2.6 Spin Momenta

We define in order to find an equation that governs the flywheel spin axis momentum

$$g = \vec{\mathbf{c}}_s \cdot \vec{\mathbf{g}}_w \tag{3.53}$$

where $\vec{\mathbf{g}}_w$ is the torque that the body imparts on the flywheel. The scalar g_{MW} represents the axial torque on the flywheel. The absolute angular momentum of any flywheel in the $\vec{\mathbf{c}}_s$ direction is

$$h_{swa} = \vec{\mathbf{c}}_s \cdot \vec{\mathbf{h}}_{wa} \tag{3.54}$$

where $\vec{\mathbf{h}}_{wa}$ is the absolute angular momentum of the flywheel. Differentiating gives

$$\dot{h}_{swa} = \dot{\vec{\mathbf{c}}}_s \cdot \vec{\mathbf{h}}_{swa} + \vec{\mathbf{c}}_s \cdot \dot{\vec{\mathbf{h}}}_{swa} \tag{3.55}$$

The time derivative of the unit vector $\vec{\mathbf{c}}_s$ is

$$\dot{\vec{\mathbf{c}}}_s = \vec{\boldsymbol{\omega}} \times \vec{\mathbf{c}}_s \tag{3.56}$$

The change in angular momentum of the flywheel can be rewritten as

$$\begin{aligned} \dot{h}_{swa} &= (\vec{\boldsymbol{\omega}} \times \vec{\mathbf{c}}_s) \cdot \vec{\mathbf{h}}_{swa} + \vec{\mathbf{c}}_s \cdot \dot{\vec{\mathbf{h}}}_{swa} && (3.57)\\ &= \vec{\boldsymbol{\omega}} \cdot (\vec{\mathbf{c}}_s \times \vec{\mathbf{h}}_{swa}) + \vec{\mathbf{c}}_s \cdot \vec{\mathbf{g}}_w && (3.58)\\ &= \vec{\boldsymbol{\omega}} \cdot \vec{\mathbf{c}}_s \times \vec{\mathbf{I}}_{sw} \cdot \vec{\boldsymbol{\omega}}_{wa} + g && (3.59) \end{aligned}$$

where

$$\vec{\boldsymbol{\omega}}_{wa} = \vec{\boldsymbol{\omega}} + \Omega \vec{\mathbf{c}}_s \tag{3.60}$$

is the absolute angular velocity of the flywheel. We write the flywheel inertia dyadic as

$$\vec{\mathbf{I}}_{sw} = I_t \vec{\mathbf{1}} + (I_s - I_t) \vec{\mathbf{c}}_s \vec{\mathbf{c}}_s \tag{3.61}$$

where I_t and I_s are the transverse and spin inertias of the flywheel. Using the previous two equations we can form the following equalities [6]

$$\vec{\boldsymbol{\omega}} \cdot \vec{\mathbf{c}}_s \times \vec{\boldsymbol{\omega}}_{wa} = 0 \tag{3.62}$$

$$\vec{\mathbf{c}}_s \times \vec{\mathbf{I}}_{sw} = I_t \vec{\mathbf{c}}_{sj} \times \vec{\mathbf{1}} \tag{3.63}$$

Equation 3.59 simplifies to describe the motion of the flywheel as

$$\dot{h}_{swa} = g \tag{3.64}$$

We use the subscript MW to denote equations that describe the momentum wheels.

$$\dot{\mathbf{h}}_{swMWa} = \mathbf{g}_{MW} \tag{3.65}$$

for all M momentum wheels.

3.3 Summary

We have presented all $6 + 2N + M$ equations necessary to describe the motion of a rigid body with N CMGs and M momentum wheels. They are

$$\dot{\mathbf{h}} = -\boldsymbol{\omega}^{\times}\mathbf{h} + \mathbf{g}_e \tag{3.66}$$

$$\dot{\mathbf{h}}_{swMWa} = \mathbf{g}_{MW} \tag{3.67}$$

$$\dot{\mathbf{h}}_{ga} = \mathrm{diag}((\mathbf{I}_t - (\mathbf{I}_{sg} + \mathbf{I}_{sw}))\mathbf{A}_s^T\boldsymbol{\omega} - \mathbf{I}_{sw}\boldsymbol{\Omega})(\mathbf{A}_t^T\boldsymbol{\omega}) + \mathbf{g}_g \tag{3.68}$$

$$\dot{\boldsymbol{\delta}} = \mathbf{I}_g^{-1}\mathbf{h}_{ga} - \mathbf{A}_g^T\boldsymbol{\omega} \tag{3.69}$$

$$\dot{\boldsymbol{\sigma}} = \mathbf{G}(\boldsymbol{\sigma})\boldsymbol{\omega} \tag{3.70}$$

where

$$\mathbf{h} = (\mathbf{I}_B + \mathbf{A}_t\mathbf{I}_t\mathbf{A}_t^T + \mathbf{A}_s\mathbf{I}_{sg}\mathbf{A}_s^T)\boldsymbol{\omega} + \mathbf{A}_s\mathbf{h}_{swa} + \mathbf{A}_g\mathbf{h}_{ga} + \mathbf{C}_s\mathbf{h}_{swMWa} \tag{3.71}$$

$$\mathbf{h}_{swa} = \mathbf{I}_{sw}\mathbf{A}_s^T\boldsymbol{\omega} + \mathbf{I}_{sw}\boldsymbol{\Omega} \tag{3.72}$$

$$\mathbf{h}_{ga} = \mathbf{I}_g\mathbf{A}_g^T\boldsymbol{\omega} + \mathbf{I}_g\dot{\boldsymbol{\delta}} \tag{3.73}$$

$$\mathbf{h}_{swMWa} = \mathbf{I}_{swMW}\mathbf{C}_s^T\boldsymbol{\omega} + \mathbf{I}_{swMW}\boldsymbol{\Omega}_{MW} \tag{3.74}$$

$$\tag{3.75}$$

Equation 3.66 describes the angular momentum of the system. Equations 3.67 & 3.68 are the control axes for the momentum wheel and CMG, respectively. The CMG gimbal angles are represented in Equation 3.69. The kinematics for the body-fixed reference frame to the inertia reference frame are described by Equation 3.70. The equations of motion are used in the derivations of control laws.

Chapter 4

Controllers

We wish to derive control strategies and control laws that will drive the spacecraft along a reference motion. This chapter presents two control strategies. The purpose of the control strategies is to take advantage of the torque amplification of the CMGs by allowing the CMGs to provide the majority of the torque required for a given reorientation. The momentum wheels correct for initial condition and tracking errors. Control Strategy I uses the CMGs in open loop control to drive the spacecraft about a reference path, with the momentum wheels implementing a closed loop control law to correct for tracking errors. The momentum wheel control laws are derived through Lyapunov and feedback linearization techniques. Control Strategy II uses both the CMGs and momentum wheels in closed loop control. A control approach that uses both types of actuators in parallel is presented. A pseudo-parallel control strategy that uses a CMG closed loop controller and Euler integration of the state errors to provide a momentum wheel feedforward control law is presented.

The chapter begins with a brief review of Lyapunov and feedback linearization control techniques. A definition of the desired maneuver follows. The tracking errors, which are the control states, are defined next. We review the gimbal rate steering law and *singularity robust* modification of Oh and Vadali [12]. We discuss Singularity Direction Avoidance presented in Refs. [4, 16] which is an improved singularity avoidance gimbal rate steering law. Discussion of the control strategies and derivation of the momentum wheel feedback control laws conclude the chapter.

4.1 Nonlinear Control Techniques

Methods for linearly controlling a nonlinear system, such as linearization of the dynamics, can perform effectively. However, the benefits of considering the nonlinear dynamics can include increased robustness, control over a larger envelope of the dynamics, control of linearly uncontrollable systems, and preservation of physical insight into the problem. Thus, we consider nonlinear control techniques. The nonlinear control techniques, Lyapunov Direct and Feedback Linearization, are briefly reviewed.

4.1.1 Lyapunov Control Laws

The derivation of a Lyapunov control law is based on Lyapunov's second method. Consider a set of differential equations $\dot{\mathbf{x}} = \mathbf{f}(\mathbf{x})$ which describe a dynamic system. The state $\mathbf{x} = \mathbf{y} - \mathbf{y}_d$ is the difference between the desired and current state. The stability of the system is analyzed by examining a scalar energy-like function of the state, $V = V(\mathbf{x})$. The desired state is globally asymptotically stable if

$$V(\mathbf{0}) = 0 \tag{4.1}$$
$$V(\mathbf{x}) > 0 \text{ for } \mathbf{x} \neq \mathbf{0} \tag{4.2}$$
$$V(\mathbf{x}) \rightarrow \infty \text{ for } \|\mathbf{x}\| \rightarrow \infty \tag{4.3}$$
$$\dot{V}(\mathbf{x}) < 0 \text{ for } \mathbf{x} \neq \mathbf{0} \tag{4.4}$$

Lyapunov control laws use the inputs of the system to ensure that the conditions for stability of the desired state are met. [37, 38]

4.1.2 Feedback Linearization

The purpose of feedback linearization is to use the inputs to cancel out the nonlinearities of the system. Linear feedback control laws can then be applied to the system to provide stability. For a continuously differentiable system $\dot{\mathbf{x}} = \mathbf{f}(\mathbf{x}, \mathbf{u})$, where $\mathbf{f}(\mathbf{0}, \mathbf{0}) = \mathbf{0}$, we want to use a state feedback controller that stabilizes the system. Note that for a system in the standard feedback linearization form,

$$\dot{\mathbf{x}} = \mathbf{A}\mathbf{x} + \mathbf{B}\boldsymbol{\beta}^{-1}(\mathbf{x})[\mathbf{u} - \boldsymbol{\alpha}(\mathbf{x})] \tag{4.5}$$

we can choose a control,

$$\mathbf{u} = \boldsymbol{\alpha}(\mathbf{x}) + \boldsymbol{\beta}(\mathbf{x})\boldsymbol{\nu} \tag{4.6}$$

that makes the closed loop dynamics,

$$\dot{\mathbf{x}} = \mathbf{A}\mathbf{x} + \mathbf{B}\boldsymbol{\nu} \tag{4.7}$$

linear. By setting $\boldsymbol{\nu} = \mathbf{K}\mathbf{x}$, and choosing gain $\mathbf{K}$ such that $\mathbf{A}+\mathbf{B}\mathbf{K}$ is Hurwitz, the closed loop system is made globally asymptotically stable. Systems that are not in the standard form can be transformed with a change of state variables since the state equations of the system are not unique. Details on the state variable transformation can be found in Refs. [37, 38, 39].

4.2 Reference Motion

We now define the motion that we want the spacecraft to track. Consider a rigid reference body that has a body-fixed reference frame $\mathcal{F}_R$. The center of mass of the reference body is coincident with the origin of $\mathcal{F}_R$ and is fixed in inertial space. The orientation of $\mathcal{F}_R$ with respect to the inertial reference frame $\mathcal{F}_I$ is expressed by the direction cosine matrix $\mathbf{R}^{RI}$ and by a set of MRPs, $\boldsymbol{\sigma}_R$. The equations that describe the motion of the reference body are

$$\dot{\mathbf{h}}_R = -\boldsymbol{\omega}_R^{\times}\mathbf{I}_B\boldsymbol{\omega}_R + \mathbf{g}_R \tag{4.8}$$

$$\dot{\boldsymbol{\sigma}}_R = \mathbf{G}(\boldsymbol{\sigma}_R)\boldsymbol{\omega}_R \tag{4.9}$$

where $\boldsymbol{\omega}_R$ is the absolute angular velocity of $\mathcal{F}_R$ and $\mathbf{g}_R$ is the external torque on the reference body. Note that the reference body has the same inertia as the controlled body but does not include the actuator inertias.

4.3 Error States

With the reference body and the spacecraft fully defined we can form the terms $\delta\boldsymbol{\sigma}$ and $\delta\boldsymbol{\omega}$ [40],

$$\delta\boldsymbol{\sigma} = \boldsymbol{\sigma} - \boldsymbol{\sigma}_R \tag{4.10}$$

$$= \frac{(1-\boldsymbol{\sigma}_R^T\boldsymbol{\sigma}_R)\boldsymbol{\sigma} - (1-\boldsymbol{\sigma}^T\boldsymbol{\sigma})\boldsymbol{\sigma}_R + 2\boldsymbol{\sigma}^{\times}\boldsymbol{\sigma}_R}{1 + (\boldsymbol{\sigma}_R^T\boldsymbol{\sigma}_R)(\boldsymbol{\sigma}^T\boldsymbol{\sigma}) + 2\boldsymbol{\sigma}_R^T\boldsymbol{\sigma}} \tag{4.11}$$

$$\delta\boldsymbol{\omega} = \boldsymbol{\omega} - \mathbf{R}^{BR}\boldsymbol{\omega}_R \tag{4.12}$$

Using these equations we define

$$\delta\mathbf{h} = \mathbf{h} - \mathbf{I}_B\mathbf{R}^{BR}\boldsymbol{\omega}_R \tag{4.13}$$

the difference between the angular momentum of the bodies, where $\mathbf{R}^{BR} = \mathbf{R}(\delta\boldsymbol{\sigma})$.

Substituting Equation 3.28 into $\delta\mathbf{h}$ and simplifying gives

$$\begin{aligned}\delta\mathbf{h} &= \mathbf{I}_B\boldsymbol{\omega} + (\mathbf{A}_t\mathbf{I}_t\mathbf{A}_t^T + \mathbf{A}_s\mathbf{I}_{sg}\mathbf{A}_s^T)\boldsymbol{\omega} + \mathbf{A}_s\mathbf{h}_{swa} + \mathbf{A}_g\mathbf{h}_{ga} \\ &\quad + \mathbf{C}_s\mathbf{h}_{swMWa} - \mathbf{I}_B\mathbf{R}^{BR}\boldsymbol{\omega}_R \qquad (4.14)\\ &= \mathbf{I}_B\delta\boldsymbol{\omega} + (\mathbf{A}_t\mathbf{I}_t\mathbf{A}_t^T + \mathbf{A}_s\mathbf{I}_{sg}\mathbf{A}_s^T)\boldsymbol{\omega} + \mathbf{A}_s\mathbf{h}_{swa} + \mathbf{A}_g\mathbf{h}_{ga} \\ &\quad + \mathbf{C}_s\mathbf{h}_{swMWa} \qquad (4.15)\end{aligned}$$

Taking the time derivative of Equation 4.13 yields

$$\delta\dot{\mathbf{h}} = \dot{\mathbf{h}} - \mathbf{I}_B\frac{d\mathbf{R}^{BR}}{dt}\boldsymbol{\omega}_R - \mathbf{I}_B\mathbf{R}^{BR}\dot{\boldsymbol{\omega}}_R \qquad (4.16)$$

Hall *et al.* [2] showed that

$$\mathbf{I}_B\frac{d\mathbf{R}^{BR}}{dt}\boldsymbol{\omega}_R = \mathbf{I}_B\boldsymbol{\omega}^{\times}\delta\boldsymbol{\omega} \qquad (4.17)$$

Taking the time derivative of Equation 4.15 gives

$$\begin{aligned}\delta\dot{\mathbf{h}} &= \mathbf{I}_B\delta\dot{\boldsymbol{\omega}} + \dot{\mathbf{A}}_s\mathbf{h}_{swa} + \mathbf{A}_s\dot{\mathbf{h}}_{swa} + \mathbf{A}_g\dot{\mathbf{h}}_{ga} + \mathbf{C}_s\dot{\mathbf{h}}_{swMWa} \qquad (4.18)\\ &\quad + (\dot{\mathbf{A}}_t\mathbf{I}_t\mathbf{A}_t^T + \mathbf{A}_t\mathbf{I}_t\dot{\mathbf{A}}_t^T + \dot{\mathbf{A}}_s\mathbf{I}_{sg}\mathbf{A}_s^T + \mathbf{A}_s\mathbf{I}_{sg}\dot{\mathbf{A}}_s^T)\boldsymbol{\omega} + (\mathbf{A}_t\mathbf{I}_t\mathbf{A}_t^T + \mathbf{A}_s\mathbf{I}_{sg}\mathbf{A}_s^T)\dot{\boldsymbol{\omega}}\end{aligned}$$

The state equations are the attitude and angular velocity error rates. We use Equation 4.18 and Equation 3.4 to express the states as

$$\begin{aligned}\delta\dot{\boldsymbol{\sigma}} &= \mathbf{G}(\delta\boldsymbol{\sigma})\delta\boldsymbol{\omega} \qquad (4.19)\\ \delta\dot{\boldsymbol{\omega}} &= \mathbf{I}_B^{-1}[\delta\dot{\mathbf{h}} - \dot{\mathbf{A}}_s\mathbf{h}_{swa} - \mathbf{A}_s\dot{\mathbf{h}}_{swa} - \mathbf{A}_g\dot{\mathbf{h}}_{ga} - (\mathbf{A}_t\mathbf{I}_t\mathbf{A}_t^T + \mathbf{A}_s\mathbf{I}_{sg}\mathbf{A}_s^T)\dot{\boldsymbol{\omega}} \qquad (4.20)\\ &\quad -(\dot{\mathbf{A}}_t\mathbf{I}_t\mathbf{A}_t^T + \mathbf{A}_t\mathbf{I}_t\dot{\mathbf{A}}_t^T + \dot{\mathbf{A}}_s\mathbf{I}_{sg}\mathbf{A}_s^T + \mathbf{A}_s\mathbf{I}_{sg}\dot{\mathbf{A}}_s^T)\boldsymbol{\omega} - \mathbf{C}_s\mathbf{g}_{MW}]\end{aligned}$$

The state equations are time invariant.

The error between the reference frame motion and the body-fixed motion has been defined. We use the tracking error as the states of our nonlinear control laws. The remainder of the chapter focuses on control laws that drive the tracking error to zero.

4.4 Control Moment Gyro Feedback Control Law

We use a gimbal rate steering law first presented by Oh and Vadali [12] to find the CMG control maneuver for a large rapid slew. Presented in this notation the gimbal torques are

$$\mathbf{g}_g = \mathbf{I}_g\ddot{\boldsymbol{\delta}} + \mathbf{I}_g\mathbf{A}_g^T\dot{\boldsymbol{\omega}} - \mathrm{diag}((\mathbf{I}_t - \mathbf{I}_s)\mathbf{A}_s^T\boldsymbol{\omega} - \mathbf{I}_{sw}\boldsymbol{\Omega})\mathbf{A}_t^T\boldsymbol{\omega} \qquad (4.21)$$

where

$$\begin{aligned}
\ddot{\boldsymbol{\delta}} &= k_\delta(\dot{\boldsymbol{\delta}}_{des} - \dot{\boldsymbol{\delta}}) && (4.22)\\
\dot{\boldsymbol{\delta}}_{des} &= \mathbf{D}^\dagger(k_3\delta\boldsymbol{\omega} + k_4\delta\boldsymbol{\sigma} - \mathbf{I}_B\mathbf{R}^{BR}\dot{\omega}_R - \mathbf{I}_B^{-1}\boldsymbol{\omega}^\times(\mathbf{I}_B\boldsymbol{\omega} + \mathbf{A}_s\mathbf{h}_{swa} + \mathbf{A}_g\mathbf{h}_{ga})) && (4.23)\\
\mathbf{D} &= -\mathbf{A}_t\mathrm{diag}(\mathbf{I}_{sw}\boldsymbol{\Omega}) && (4.24)\\
&\quad +1/2[(\mathbf{a}_{s1}\mathbf{a}_{t1}^T + \mathbf{a}_{t1}\mathbf{a}_{s1}^T)(\boldsymbol{\omega} + \mathbf{R}^{BR}\boldsymbol{\omega}_R)\,(\mathbf{a}_{s2}\mathbf{a}_{t2}^T + \mathbf{a}_{t2}\mathbf{a}_{s2}^T)(\boldsymbol{\omega} + \mathbf{R}^{BR}\boldsymbol{\omega}_R)...\\
&\quad ...(\mathbf{a}_{sN}\mathbf{a}_{tN}^T + \mathbf{a}_{tN}\mathbf{a}_{sN}^T)(\boldsymbol{\omega} + \mathbf{R}^{BR}\boldsymbol{\omega}_R)](\mathbf{I}_t - \mathbf{I}_s)
\end{aligned}$$

The † denotes the pseudo-inverse. The coefficients k_δ, k_3, and k_4 are positive constant scalars [4].

4.4.1 Singularity Avoidance

Special configurations of the CMG gimbal angles can result in singularities where the CMG cluster cannot provide torque in a specified direction. To avoid singular configurations we use a *singularity-robust steering law* [12]. For simplicity we rewrite equation 4.23 as

$$\dot{\boldsymbol{\delta}}_{des} = \mathbf{D}^\dagger \mathrm{L}_r \tag{4.25}$$

Unreasonable gimbal rates are produced when $\mathbf{D}$ becomes close to singular. We modify equation 4.25 to be

$$\dot{\boldsymbol{\delta}}_{des} = \mathbf{D}^T(\mathbf{D}\mathbf{D}^T + \alpha\mathbf{1})^{-1}\mathrm{L}_r \tag{4.26}$$

where

$$\alpha = \alpha_0 \exp^{-\det(\mathbf{D}\mathbf{D}^T)} \tag{4.27}$$

is a scalar parameter that increases as a singularity configuration is approached. The coefficient α_0 is a small constant [12].

4.4.2 Singular Direction Avoidance

An improvement to *singularity-robust steering law* [12] called *Singular Direction Avoidance* was presented by Ford and Hall [4, 16]. *Singular Direction Avoidance* is based on the singular value decomposition to compute the pseudo inverse in order to steer the CMGs away from singular configurations. Ford and Hall proved that the torque error from singularity avoidance was always less with *Singular Direction Avoidance* than with *singularity-robust steering law* [4, 16].

We modify Equation 4.27 to be

$$\alpha = \alpha_0 \exp^{-k_{SDA}\sigma_{33}^2} \tag{4.28}$$

where

$$\sigma_{33}^2 = \sqrt{3/N}\mathbf{S}(3,3)/h_{swr} \tag{4.29}$$

The number of CMGs in the spacecraft is N. The matrix $\mathbf{S}$ is found through the singular value decomposition problem. For the general $m \times n$ matrix $\mathbf{D}$ can be decomposed into a product of three matrices

$$\mathbf{D} = \mathbf{U}\mathbf{S}\mathbf{V}^T \tag{4.30}$$

where $\mathbf{U}$ is an $m \times m$ unitary matrix,$\mathbf{V}$ is an $n \times n$ unitary matrix, and $\mathbf{S}$ is an $m \times n$ diagonal matrix. Equation 4.26 becomes

$$\dot{\boldsymbol{\delta}}_{des} = \mathbf{V}\mathbf{S}\mathbf{U}^T\mathrm{L}_r \tag{4.31}$$

where

$$\mathbf{S} = \mathrm{diag}(1/S_{11}, 1/S_{22}, S_{33}/(S_{33}^2 + \alpha)) \tag{4.32}$$

We perform numerical simulations of *Singular Direction Avoidance* versus *singularity-robust* to illustrate its benefits. For the majority of the simulations that involve mixed attitude control strategies we use the *singularity-robust steering law.*

4.5 Control Strategy I: Open Loop Control Moment Gyro with Closed Loop Momentum Wheel Control

The first strategy requires prerequisite knowledge of the reorientation or reference motion. Numerical simulation of the CMG gimbal rate steering law for the given reference motion are performed. The gimbal angle, velocity, and acceleration for the maneuver are found from the numerical simulation. The gimbal information is implemented on the spacecraft in an open loop form. With zero initial condition error and perfect knowledge of the system the open loop CMG maneuver will force the spacecraft along the desired reference motion. However, initial condition errors, perturbations, and/or system parameter uncertainty will cause the spacecraft to diverge from the reference motion. Implementation of the derived momentum wheel feedback control laws correct for initial condition errors and perturbations. Figure 4.1 shows a block diagram of the control strategy. The 'Reference Motion' block symbolizes the angular velocity and attitude for the desired maneuver. The 'System' block represents the spacecraft's angular velocity and attitude. The output of the system is the difference between the reference and system angular velocity and attitude. The CMG gimbal information from the preprocessed maneuver is passed to the spacecraft in open loop. The momentum wheel feedback control

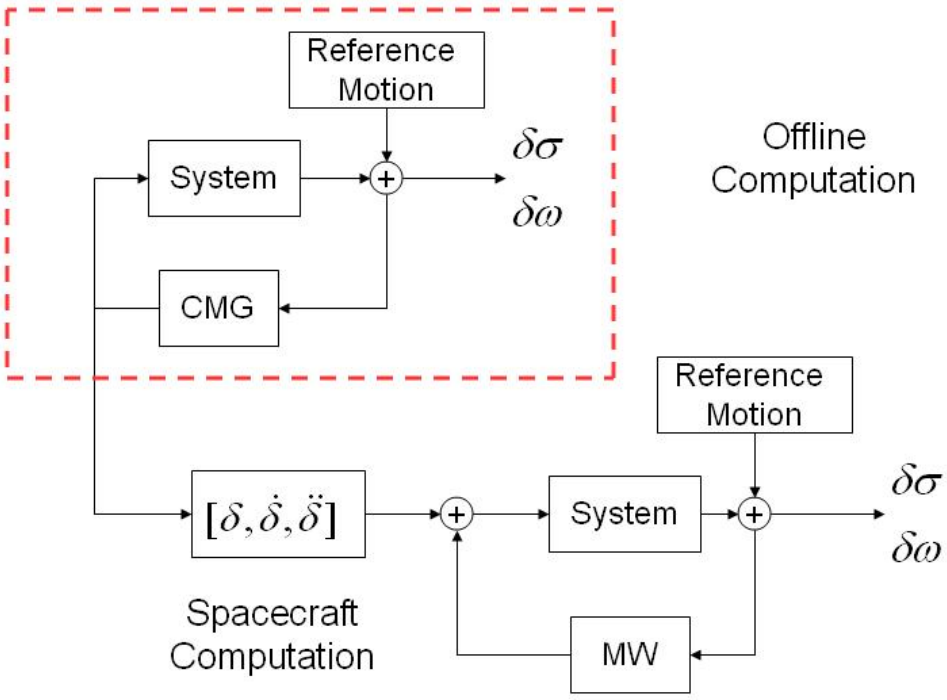

Figure 4.1: *Control Organization for CMG Open Loop and Momentum Wheel Closed Loop Control*

compensates for any initial condition or tracking error between the reference trajectory and the real spacecraft. Note that the majority of the torque required for the maneuver still comes from the CMGs, and not the momentum wheels.

4.5.1 Momentum Wheel Lyapunov Control

A Lyapunov Control law is derived to minimize tracking error of the body fixed reference frame to reference frame. Using Lyapunov's method a feedback control laws is derived.

Consider a Lyapunov candidate function

$$V = \frac{1}{2}\delta\boldsymbol{\omega}^T\mathbf{K}_1\delta\boldsymbol{\omega} + 2k_2\ln(1+\delta\boldsymbol{\sigma}^T\delta\boldsymbol{\sigma}) \tag{4.33}$$

where $\mathbf{K}_1 = \mathbf{K}_1^T > 0$ and $k_2 > 0$. The derivative of V is

$$\dot{V} = \dot{\mathbf{H}}^T\mathbf{I}_B^{-1}\mathbf{K}_1\delta\boldsymbol{\omega} + k_2\delta\boldsymbol{\sigma}^T\delta\boldsymbol{\omega} \tag{4.34}$$

where

$$\begin{aligned}\dot{\mathbf{H}} &= \delta\dot{\mathbf{h}} - \dot{\mathbf{A}}_s\mathbf{h}_{swa} - \mathbf{A}_s\dot{\mathbf{h}}_{swa} - \mathbf{C}_s\dot{\mathbf{h}}_{swMWa} - \mathbf{A}_g\dot{\mathbf{h}}_{ga} \\ &\quad -(\dot{\mathbf{A}}_t\mathbf{I}_t\mathbf{A}_t^T + \mathbf{A}_t\mathbf{I}_t\dot{\mathbf{A}}_t^T + \dot{\mathbf{A}}_s\mathbf{I}_{sg}\mathbf{A}_s^T + \mathbf{A}_s\mathbf{I}_{sg}\dot{\mathbf{A}}_s^T)\boldsymbol{\omega} \\ &\quad -(\mathbf{A}_t\mathbf{I}_t\mathbf{A}_t^T + \mathbf{A}_s\mathbf{I}_{sg}\mathbf{A}_s^T)\dot{\boldsymbol{\omega}}\end{aligned} \tag{4.35}$$

Equation 4.35 can be expanded to

$$\begin{aligned}\dot{\mathbf{H}} &= -\boldsymbol{\omega}^\times((\mathbf{I}_B + \mathbf{A}_t\mathbf{I}_t\mathbf{A}_t^T + \mathbf{A}_s\mathbf{I}_{sg}\mathbf{A}_s^T)\boldsymbol{\omega} + \mathbf{A}_s\mathbf{h}_{swa} + \mathbf{A}_g\mathbf{h}_{ga} \\ &\quad +\mathbf{C}_s\mathbf{h}_{swMWa}) + \mathbf{g}_e - \mathbf{I}_B\boldsymbol{\omega}^\times\delta\boldsymbol{\omega} - \mathbf{I}_B\mathbf{R}^{BR}\mathbf{I}_B^{-1}[-\boldsymbol{\omega}_R^\times\mathbf{I}\boldsymbol{\omega}_R + \mathbf{g}_R] \\ &\quad -\dot{\mathbf{A}}_s\mathbf{h}_{swa} - \mathbf{A}_s\mathbf{g}_w - \mathbf{C}_s\mathbf{g}_{MW} \\ &\quad -\mathbf{A}_g(\mathrm{diag}((\mathbf{I}_t - \mathbf{I}_s)\mathbf{A}_s^T\boldsymbol{\omega} - \mathbf{I}_{sw}\boldsymbol{\Omega})(\mathbf{A}_t^T\boldsymbol{\omega}) + \mathbf{g}_g) \\ &\quad -(\dot{\mathbf{A}}_t\mathbf{I}_t\mathbf{A}_t^T + \mathbf{A}_t\mathbf{I}_t\dot{\mathbf{A}}_t^T + \dot{\mathbf{A}}_s\mathbf{I}_{sg}\mathbf{A}_s^T + \mathbf{A}_s\mathbf{I}_{sg}\dot{\mathbf{A}}_s^T)\boldsymbol{\omega} \\ &\quad -(\mathbf{A}_t\mathbf{I}_t\mathbf{A}_t^T + \mathbf{A}_s\mathbf{I}_{sg}\mathbf{A}_s^T)\dot{\boldsymbol{\omega}}\end{aligned} \tag{4.36}$$

With $\dot{\mathbf{H}}$ in expanded form we identify the control torques for the system $\mathbf{g}_e$, $\mathbf{g}_w$, $\mathbf{g}_g$, and $\mathbf{g}_{MW}$. The spin torque for a CMG to maintain a constant velocity of the flywheel about its spin axis relative to the body is

$$\mathbf{g}_w = \mathbf{I}_{sw}(\dot{\mathbf{A}}_s^T\boldsymbol{\omega} + \mathbf{A}_s^T\dot{\boldsymbol{\omega}}) \tag{4.37}$$

For this problem we consider $\mathbf{g}_e$, $\mathbf{g}_w$, and $\mathbf{g}_g$ as known parameters. With the $\mathbf{g}_{MW}$ input we can insure that the conditions for global asymptotic stability, Equations 4.1, 4.2, 4.3, 4.4, are met.

By choosing $\mathbf{K}_1 = \mathbf{I}_B$ equation 4.34 becomes

$$\dot{V} = \delta\boldsymbol{\omega}^T(\dot{\mathbf{H}} + k_2\delta\boldsymbol{\sigma}) \tag{4.38}$$

We choose the control torque $\mathbf{g}_{MW}$ to be

$$\begin{aligned}\mathbf{C}_s\mathbf{g}_{MW} &= \delta\dot{\mathbf{h}} - \dot{\mathbf{A}}_s\mathbf{h}_{swa} - \mathbf{A}_s\mathbf{g}_w - \mathbf{A}_g\dot{\mathbf{h}}_{ga} - (\mathbf{A}_t\mathbf{I}_t\mathbf{A}_t^T + \mathbf{A}_s\mathbf{I}_{sg}\mathbf{A}_s^T)\dot{\boldsymbol{\omega}} \\ &\quad -(\dot{\mathbf{A}}_t\mathbf{I}_t\mathbf{A}_t^T + \mathbf{A}_t\mathbf{I}_t\dot{\mathbf{A}}_t^T + \dot{\mathbf{A}}_s\mathbf{I}_{sg}\mathbf{A}_s^T + \mathbf{A}_s\mathbf{I}_{sg}\dot{\mathbf{A}}_s^T)\boldsymbol{\omega} \\ &\quad +k_2\delta\boldsymbol{\sigma} + k_1\delta\boldsymbol{\omega}\end{aligned} \tag{4.39}$$

which yields

$$\dot{V} = -k_1\delta\boldsymbol{\omega}^T\delta\boldsymbol{\omega} \leq 0 \tag{4.40}$$

since $k_1 > 0$. From this result we see that

$$\lim_{t\to\infty}\delta\boldsymbol{\omega}(t) = 0 \tag{4.41}$$

Substituting the control input Equation 4.39 into the state equation $\delta\dot{\boldsymbol{\omega}}$, we have

$$\mathbf{I}_B\delta\dot{\boldsymbol{\omega}} = -k_2\delta\boldsymbol{\sigma} - k_1\delta\boldsymbol{\omega} \tag{4.42}$$

Due to Equation 4.41 we have

$$\lim_{t\to\infty}\mathbf{I}_B\delta\dot{\boldsymbol{\omega}} = -\lim_{t\to\infty}k_2\delta\boldsymbol{\sigma} \tag{4.43}$$

so that $\delta\boldsymbol{\sigma}\to 0$. From Equation 4.19 we know that $\delta\dot{\boldsymbol{\sigma}}\to 0$, therefore the limit of $\delta\boldsymbol{\sigma}$ is a constant, thus

$$\lim_{t\to 0}\delta\boldsymbol{\sigma} = 0 \tag{4.44}$$

With LaSalle's Invariance Principle [37], the attitude and angular velocity error due to tracking with this control law is globally asymptotically stable.

4.5.2 Momentum Wheel Lyapunov Control with Constant Moment of Inertia Assumption

For most systems the change in inertia due to the CMGs is orders of magnitude smaller than the system inertia. We can reduces the amount of computation required by the controller if we assume that the change in the moment of inertia of the system due to the CMGs is negligible. The state equations are

$$\delta\dot{\boldsymbol{\sigma}} = \mathbf{G}(\delta\boldsymbol{\sigma})\delta\boldsymbol{\omega} \tag{4.45}$$

$$\begin{aligned}\delta\dot{\boldsymbol{\omega}} = \mathbf{I}_B^{-1}[&\delta\dot{\mathbf{h}} - \dot{\mathbf{A}}_s\mathbf{h}_{swa} - \mathbf{A}_s\dot{\mathbf{h}}_{swa} - \mathbf{A}_g\dot{\mathbf{h}}_{ga} - (\mathbf{A}_t\mathbf{I}_t\mathbf{A}_t^T + \mathbf{A}_s\mathbf{I}_{sg}\mathbf{A}_s^T)\dot{\boldsymbol{\omega}} \\ &-\mathbf{C}_s\mathbf{g}_{MW}]\end{aligned} \tag{4.46}$$

Using the Lyapunov candidate function of Equation 4.33 a control input of

$$\begin{aligned}\mathbf{C}_s\mathbf{g}_{MW} = &\delta\dot{\mathbf{h}} - \dot{\mathbf{A}}_s\mathbf{h}_{swa} - \mathbf{A}_s\mathbf{g}_w - \mathbf{A}_g\dot{\mathbf{h}}_{ga} - (\mathbf{A}_t\mathbf{I}_t\mathbf{A}_t^T + \mathbf{A}_s\mathbf{I}_{sg}\mathbf{A}_s^T)\dot{\boldsymbol{\omega}} \\ &+k_2\delta\boldsymbol{\sigma} + k_1\delta\boldsymbol{\omega}\end{aligned} \tag{4.47}$$

globally asymptotically stabilizes the desired state.

4.5.3 Momentum Wheel Lyapunov Control Without Knowledge of the CMGs

To save computation time we consider the previous Lyapunov control laws without knowledge of the CMGs. Equation 4.18 becomes

$$\delta\dot{\mathbf{h}} = \mathbf{I}_B\delta\dot{\boldsymbol{\omega}} + \mathbf{C}_s\mathbf{h}_{swMWa} \tag{4.48}$$

The time derivative of the angular velocity error Equation 4.20 becomes

$$\delta\dot{\boldsymbol{\omega}} = \mathbf{I}_B^{-1}[\delta\dot{\mathbf{h}} - \mathbf{C}_s\mathbf{g}_{MW}] \tag{4.49}$$

The candidate Lyapunov function remains in the same form as Equation 4.33 where $\mathbf{K}_1 = \mathbf{K}_1^T > 0$ and $k_2 > 0$. The time derivative of the candidate Lyapunov function is

$$\dot{V} = \delta\boldsymbol{\omega}^T(\delta\dot{\mathbf{h}} - \mathbf{C}_s\dot{\mathbf{h}}_{swMWa} + k_2\delta\boldsymbol{\sigma}) \tag{4.50}$$

where we have chosen $\mathbf{K}_1 = \mathbf{I}_B$. Clearly by choosing

$$\mathbf{C}_s\mathbf{g}_{MW} = \delta\dot{\mathbf{h}} + k_2\delta\boldsymbol{\sigma} + k_1\delta\boldsymbol{\omega} \tag{4.51}$$

the system will be globally asymptotically stable given the previous LaSalle's Invariance Principal discussion.

4.5.4 Momentum Wheel Feedback Linearization

We now take a different approach to feedback control. For a certain class of nonlinear systems we can use a change of variables and state feedback control that transforms the nonlinear system into a linear system [37]. We investigate input-state linearization of this nonlinear system.

We begin with the state equations 4.19 and 4.20 which we transform with

$$\mathbf{z}_1 = \delta\boldsymbol{\sigma} \tag{4.52}$$
$$\mathbf{z}_2 = \mathbf{G}(\delta\boldsymbol{\sigma})\delta\boldsymbol{\omega} = \delta\dot{\boldsymbol{\sigma}} \tag{4.53}$$

The transformed state equations are

$$\dot{\mathbf{z}}_1 = \mathbf{z}_2 \tag{4.54}$$
$$\dot{\mathbf{z}}_2 = \dot{\mathbf{G}}\delta\boldsymbol{\omega} + \mathbf{G}\delta\dot{\boldsymbol{\omega}} \tag{4.55}$$

where $\dot{\mathbf{G}} = \mathbf{G}(\delta\dot{\boldsymbol{\sigma}})$. Substitution of Equation 4.20 allows the state equations to be written as

$$\dot{\mathbf{z}}_1 = \mathbf{z}_2 \tag{4.56}$$
$$\begin{aligned}\dot{\mathbf{z}}_2 = {} & \dot{\mathbf{G}}\delta\boldsymbol{\omega} + \mathbf{G}(\mathbf{I}_B^{-1}(\delta\dot{\mathbf{h}} - \dot{\mathbf{A}}_s\mathbf{h}_{swa} - \mathbf{A}_s\dot{\mathbf{h}}_{swa} - \mathbf{A}_g\dot{\mathbf{h}}_{ga} \\ & -(\dot{\mathbf{A}}_t\mathbf{I}_t\mathbf{A}_t^T + \mathbf{A}_t\mathbf{I}_t\dot{\mathbf{A}}_t^T + \dot{\mathbf{A}}_s\mathbf{I}_{sg}\mathbf{A}_s^T + \mathbf{A}_s\mathbf{I}_{sg}\dot{\mathbf{A}}_s^T)\boldsymbol{\omega} \\ & -(\mathbf{A}_t\mathbf{I}_t\mathbf{A}_t^T + \mathbf{A}_s\mathbf{I}_{sg}\mathbf{A}_s^T)\dot{\boldsymbol{\omega}} - \mathbf{C}_s\mathbf{g}_{MW})\end{aligned} \tag{4.57}$$

In this form we can choose $\mathbf{C}_s\mathbf{g}_{MW}$ to cancel the nonlinear terms. We choose the momentum wheel control torques to be

$$\begin{aligned}\mathbf{C}_s\mathbf{g}_{MW} &= \delta\dot{\mathbf{h}} - \dot{\mathbf{A}}_s\mathbf{h}_{swa} - \mathbf{A}_s\dot{\mathbf{h}}_{swa} - \mathbf{A}_g\dot{\mathbf{h}}_{ga} \\ &\quad -(\dot{\mathbf{A}}_t\mathbf{I}_t\mathbf{A}_t^T + \mathbf{A}_t\mathbf{I}_t\dot{\mathbf{A}}_t^T + \dot{\mathbf{A}}_s\mathbf{I}_{sg}\mathbf{A}_s^T + \mathbf{A}_s\mathbf{I}_{sg}\dot{\mathbf{A}}_s^T)\boldsymbol{\omega} \\ &\quad -(\mathbf{A}_t\mathbf{I}_t\mathbf{A}_t^T + \mathbf{A}_s\mathbf{I}_{sg}\mathbf{A}_s^T)\dot{\boldsymbol{\omega}} + \mathbf{I}_B\mathbf{G}^{-1}(\dot{\mathbf{G}}\delta\boldsymbol{\omega} + \boldsymbol{\nu})\end{aligned} \tag{4.58}$$

where

$$\boldsymbol{\nu} = k_5\delta\boldsymbol{\omega} + k_6\delta\boldsymbol{\sigma} \tag{4.59}$$

The constants k_5 and k_6 are positive. The system with control is

$$\dot{\mathbf{z}} = \begin{bmatrix} k_6 & 0 \\ 0 & k_5\mathbf{G}^{-1} \end{bmatrix}\mathbf{z} \tag{4.60}$$

With the linear closed loop system we can use linear stability analysis. From linear theory we can guarantee asymptotic stability if the coefficient matrix is Hurwitz[37].

4.5.5 One Open Loop CMG and Momentum Wheel Feedback Control

We now consider using one CMG to provide large torques about a single axis, while a cluster of momentum wheels provide closed loop attitude control. Any of the previously derived closed loop momentum wheel control laws can be used in this configuration since the stability of the closed loop system comes from the momentum wheel control laws. The advantage of this configuration is in the savings in physical hardware. The spacecraft would not require the typical 3 or 4 CMG cluster for attitude control.

Since there is an open loop portion of the controller, prior knowledge of the reference motion is still required. The calculation of the open loop CMG commands can be simplified. The desired output torque from the CMG is about the transverse axis. The output torque is $I_{sw}\Omega\sin\delta/\Delta t$, where Δt is the time to complete the gimbal angle. A more detailed discussion of the CMG output torque is in Chapter 6.

For a given reference motion we choose the CMG maneuver such that the output torque of the CMG provides much of the required torque for tracking. A simple example is to use the CMG to provide torque for a principal axis slew of the spacecraft, while the momentum wheel correct for the tracking errors. We use this example and actuator configuration on the spacecraft simulator. The simulator results are presented in Chapter 6.

4.6 Control Strategy II: Control Moment Gyro and Momentum Wheel Closed Loop Control

The second control strategy implements both the CMGs and momentum wheels in closed loop control. Figure 4.2 shows the CMG and momentum wheel control laws in a parallel

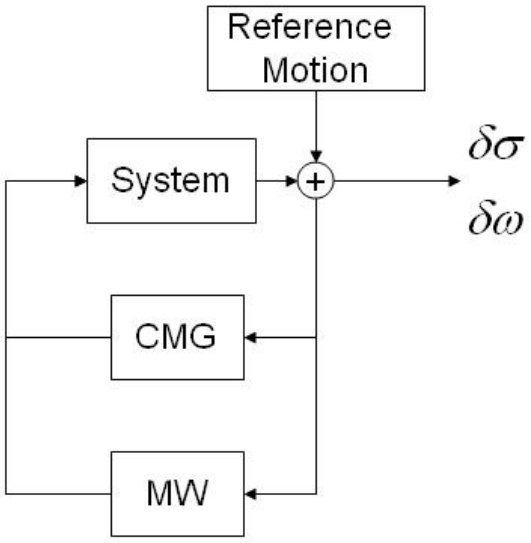

Figure 4.2: *Control Organization for CMG and Momentum Wheel Closed Loop Control*

feedback form. Implementation of multiple control laws in parallel can cause undesirable effects in performance. A possible solution for implementing two control laws is to use the CMGs with a closed loop control law, while performing an integration step forward on the errors with the commanded CMG as inputs to find a momentum wheel feedforward control torque from the predicted errors. Figure 4.3 shows a block diagram of the control strategy.

4.6.1 Parallel Control Moment Gyro and Momentum Wheel Control

For a given maneuver we want to use the tracking error without preprocessing to implement feedback control with both actuators. To this end we use the gimbal rate steering law of Section 4.3 and the Lyapunov momentum wheel control of Section 4.5.1. Independently both of these controllers have been proven to globally asymptotically stabilize

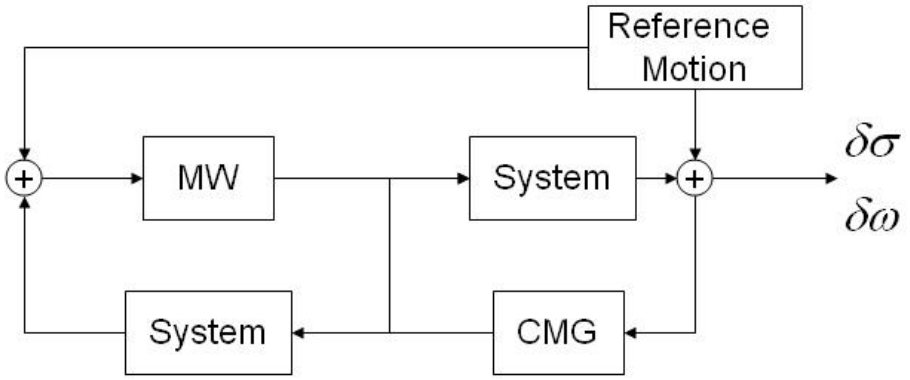

Figure 4.3: *Control Organization for CMG and Momentum Wheel Closed Loop Control*

the system.

To decrease controller computations we withhold knowledge of the CMGs from the Lyapunov momentum wheel controller. The gimbal rate steering law and Equation 4.51 are implemented in parallel. We will call this control scheme a parallel CMG and independent momentum wheel controller in later results.

4.6.2 Control Moment Gyro Closed Loop Control with Lyapunov Feedforward Momentum Wheel Control

The gimbal rate steering law is again implemented with the state errors. The CMG gimbal rate steering feedback control law generates control torques that stabilize the system. At every time step the system with the CMG control is propagated forward one time step with Euler integration. The result is a predicted error for the next time step. A Lyapunov control law uses the predicted error to calculate momentum wheel torques that will correct for the predicted error. The momentum wheel torques derived from the predicted error and the CMG torques derived from the current error are implemented together.

4.7 Summary

A closed loop CMG gimbal rate steering law is used to find open loop commands for spacecraft reorientations. The gimbal rate steering law introduces errors to tracking

by neglecting the effects of gimbal acceleration with the gimbal inertia. With perfect knowledge of the system the tracking errors are minimal. Momentum wheel closed loop control laws attempt to reject undesirable gimbal torques and initial condition errors.

Using the CMGs in open loop with prerequisite knowledge of the maneuver can be restrictive on time and generally impractical for a real spacecraft. The open loop CMG commands have to be stored in a table which the processor must continually query. Also the maneuver must be preprocessed in order to calculate the open loop CMG commands. Under ideal conditions the time lag between receiving a reference motion and execution of the maneuver might be acceptable. However, the inherit slowness of this strategy might make it unsuitable for mission goals that require large rapid slewing. A possible solution is to simplify the preprocessing by reducing the number of CMGs. Aligning the output torque of a single CMG to provide large slew torques with momentum wheel feedback can reduce time lag.

With use of Euler integration of the system with knowledge of the gimbal control torques to be applied, the attitude and angular velocity error can be predicted for the next time step. Lyapunov momentum wheel control uses the predicted error to calculate the required torques which are implemented in feedforward fashion.

Chapter 5

Numerical Simulation

We present the results of numerical simulations of the derived control laws for illustration. We first present the reference motion to be tracked. The CMG gimbal rate steering law demonstrates convergence without initial condition errors. We then show how implementing the CMG maneuver from preprocessing with slight variations in initial conditions make the system diverge (as expected) from the desired reference conditions. Implementation of the closed loop momentum wheel control laws from Strategy I show that tracking errors are rejected with minimal torques. Simulation results are shown for the parallel CMG/independent momentum wheel and the CMG feedback/momentum wheel feedforward control laws.

A trend analysis is performed to investigate the control effort variation with respect to the reference slew rate. Two controllers from Control Strategy I and II are evaluated. A quantification of the control effort required for a maneuver is presented. The control effort-like-measure is compared for simulations with and without initial condition errors. Plots of maximum control torques for each maneuver and controller with and without initial condition errors illustrate the differences between the controllers.

For all the results the time units are seconds. The angular rate units are rad/sec. The external and control torque units are $\mathrm{N} \cdot \mathrm{m}$.

5.1 System Parameters

We define the actuator orientations in $\mathcal{F}_B$ which is aligned with the principal inertia reference frame. A three-CMG configuration is aligned such that

$$\mathbf{A}_{s0} = \begin{bmatrix} 1 & 0 & 0 \\ 0 & 1 & 0 \\ 0 & 0 & 1 \end{bmatrix} \tag{5.1}$$

$$\mathbf{A}_{g} = \begin{bmatrix} 0 & -1 & 0 \\ 0 & 0 & -1 \\ -1 & 0 & 0 \end{bmatrix} \tag{5.2}$$

For simplicity we choose the initial spin axes of the CMGs to be aligned with the principal inertia axes of the body.

Table 5.1: Spacecraft Parameters

	Value	Units
$\mathbf{I}_B$	$\text{diag}(6, 5, 10)$	kg m^2
I_{sw}	0.01	kg m^2
I_{sg}	0.01	kg m^2
I_t	0.01	kg m^2
I_g	0.01	kg m^2
I_{swMW}	0.04	kg m^2
Ω	209.4	rad/s
Ω_{MW}	0	rad/s

Table 5.1 shows the CMG, momentum wheel, and body parameters. All three CMGs have the same inertia properties. The three momentum wheel spin axes are aligned with the principal axes. The transverse inertias of the momentum wheels along with inertias of the torque devices for the momentum wheels are included in the body inertia. The constants and gains for the controllers are in Table 5.2.

5.2 Reference Motion

The reference motion to be tracked is a 90^o slew about the $\hat{b}_3$ axis of $\mathcal{F}_R$. The reference motion is generated with bang-bang external torques to simulate the motion of an optimal

Table 5.2: Constants and Gains

Control Gains	
k_0	100
k_δ	100
k_1	54
k_2	47
k_3	54
k_4	47
k_5	5
k_6	4
α_0	0.01

maneuver. The external torque applied is $1\text{N} \cdot \text{m}$ for 4 seconds each in both directions. The Modified Rodrigues Parameter representation of the reorientation of the reference body is shown in Figure 5.1.

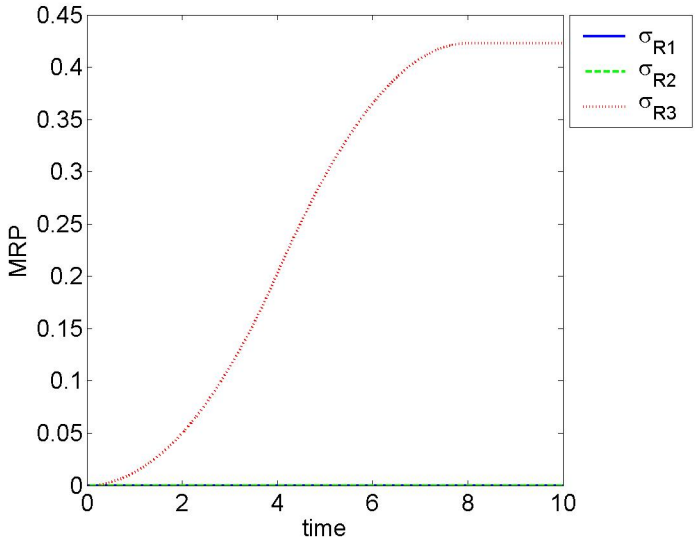

Figure 5.1: *Reference Maneuver to be Tracked*

5.3 Control Moment Gyro Gimbal Rate Steering Results

The gains for determining the control moment gyro maneuvering for the reorientation are in Table 5.2. Figure 5.2 shows the attitude and velocity error for the body with CMG feedforward control with no initial errors. The system tracks the reference motion with small errors caused by the gimbal inertias and accelerations, which are a consequence of the gimbal rate steering law. The same CMG maneuver that produced the results from Figure 5.2 is implemented with small errors in initial attitude. Figure 5.3 shows the feedforward CMG control with an initial error of $\boldsymbol{\sigma} = [0.02, 0.01, -0.01]^T$. Clearly without feedback control, any initial error or perturbation will result in errors in tracking and final orientation.

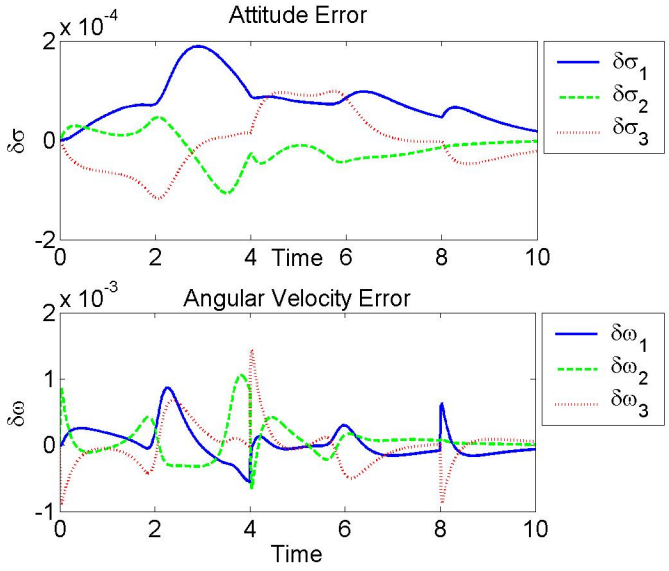

Figure 5.2: *Tracking Reference Body with CMG Feedback*

5.4 Control Strategy I Results

We have shown that the open loop CMG controller is unstable in the presence of initial errors. Control Strategy I uses closed loop momentum wheel control laws to compensate for tracking errors caused by initial conditions and singularity avoidance. We numerically simulate the controllers of Section 4.5.

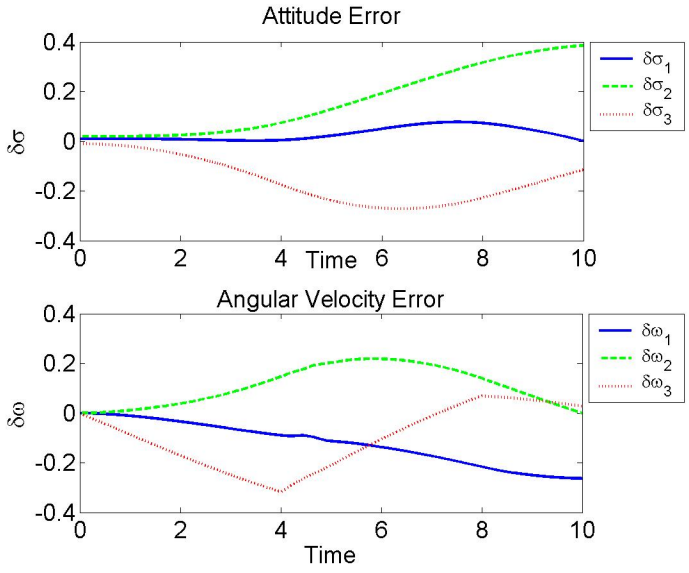

Figure 5.3: *Tracking Reference Body with CMG Feedforward*

5.4.1 Lyapunov Feedback Control

We apply the Lyapunov momentum wheel feedback control laws using the gains in Table 5.2. Figure 5.4 shows that the momentum wheels correct for initial error while allowing the majority of the torque for the slew to come from the CMGs. The attitude error decreases throughout the maneuver. The angular velocity error must be non-zero for the attitude error to converge to zero. The momentum wheel torques throughout the maneuver are also shown.

5.4.2 Lyapunov Feedback Control Ignoring ΔI

In Figure 5.5 numerical results from the same Lyapunov controller are shown ignoring the changing moment of inertia of the system due to the CMG gimbal angles. There is no major sacrifice in convergence to the reference motion compared to the Lyapunov control with changing inertia; however, there is an increase in control effort to the momentum wheels. There is a savings in computational effort by ignoring the changing moment of inertia. The trade-off is increasing the momentum wheel control effort.

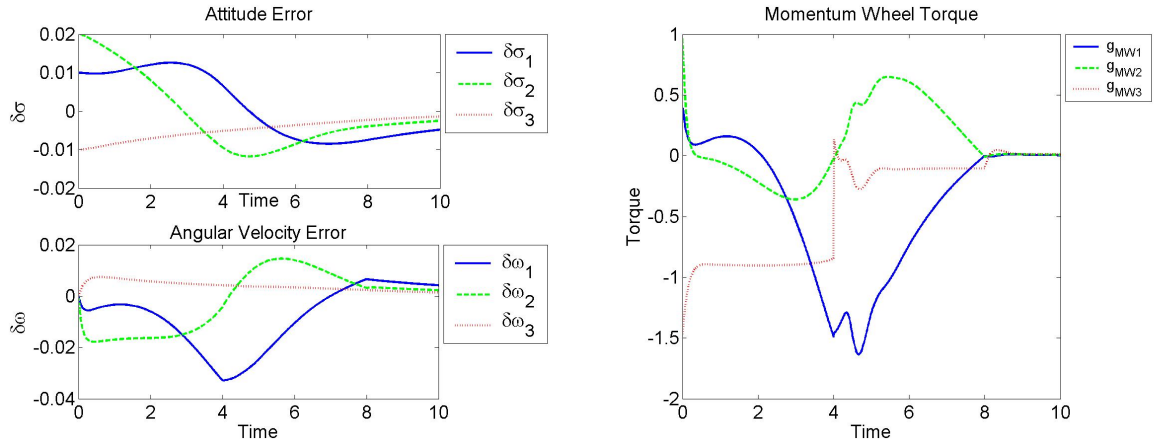

Figure 5.4: *Tracking Reference Body with CMG Feedforward and Momentum Wheel Lyapunov Feedback Control*

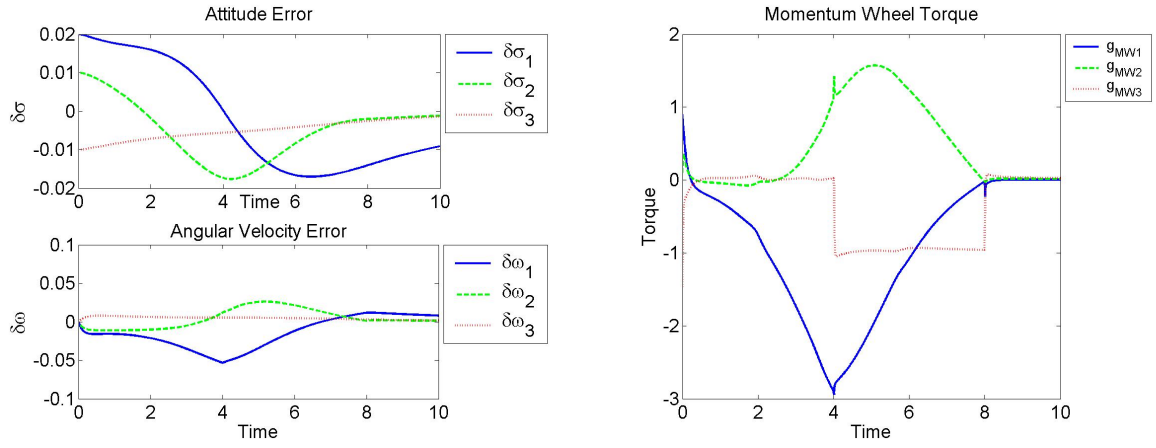

Figure 5.5: *CMG Open Loop with Lyapunov Momentum Wheel Feedback Neglecting* $d\mathbf{I}/dt$

5.4.3 Lyapunov Feedback Control without CMG Knowledge

In an effort to reduce computation time we remove knowledge of the CMGs from the momentum wheel controller. The results of the CMG open loop and independent momentum wheel closed loop control are presented in Figure 5.6. The shape of the control effort for the momentum wheels is similar to the controller that ignores the changing inertias, which is clearly disregarded by this controller too. The momentum wheel control effort is less than that of the Lyapunov controller that assumed constant inertias for the spacecraft and actuators. The system converges slower with the independent momen-

tum wheel control laws; however the magnitude of the errors is less. Convergence is still attained.

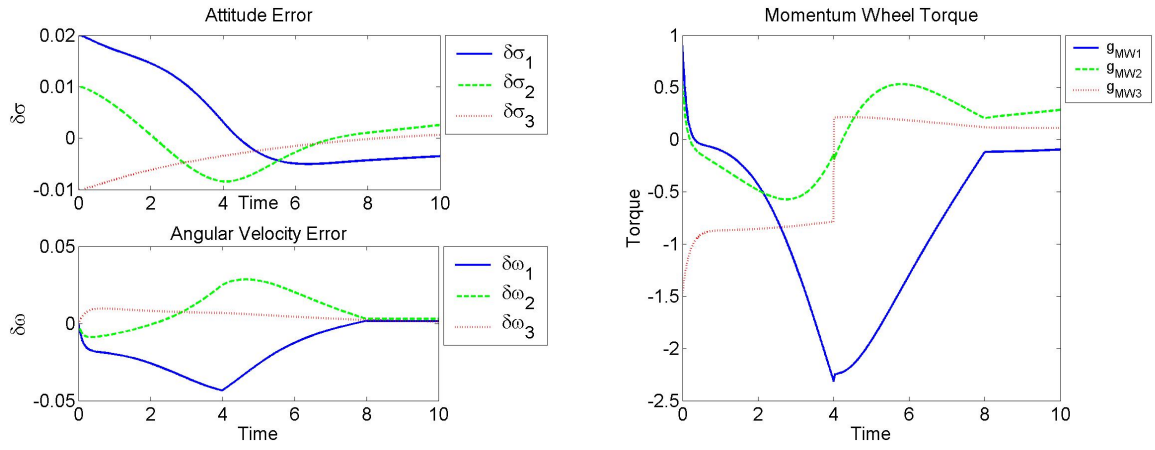

Figure 5.6: *CMG Open Loop with Independent Lyapunov Momentum Wheel Feedback*

5.4.4 Momentum Wheel Feedback Linearization

The feedback linearization control law yields the results shown in Figure 5.7. The linear gains are shown in Table 5.2. Figure 5.7 is the tracking error and momentum wheel control torques for the system. The system converges so quickly that the errors are almost null by the end of the maneuver. The momentum wheel torques required are small compared to the Lyapunov control laws of this section.

5.4.5 One CMG with Momentum Wheel Feedback Control

Recall that we can use any of the previously defined momentum wheel feedback control laws with one CMG. We choose to use the Lyapunov controller of Section 5.4.1. We choose the CMG to be initially aligned such that $\mathbf{A}_s = [1,0,0]^T$, $\mathbf{A}_t = [0,0,1]^T$, and $\mathbf{A}_g = [0,1,0]^T$. We choose this initial alignment so that the output torque of the CMG is aligned with the torque required for the reference maneuver. In a real system we could either use the momentum wheels to align the CMG optimally, or use optimal control techniques to determine the control inputs to the actuators.

The CMG gimbals to 28° in 4 seconds, then back to 0° in 4 seconds. Figure 5.8 shows the angular velocity and attitude error for the system with one CMG and the three orthogonal

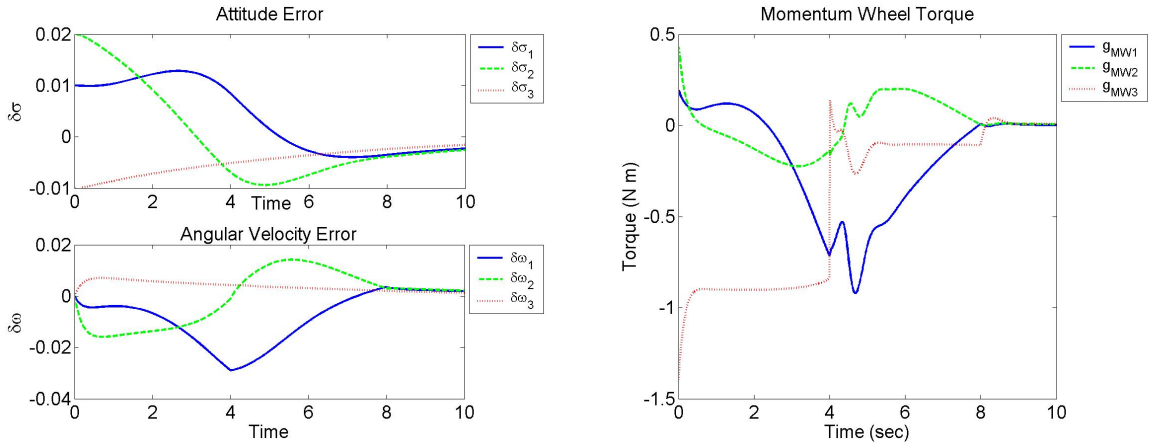

Figure 5.7: *CMG Feedforward and Momentum Wheel Feedback Linearization*

momentum wheels. The flaw with this control configuration is that the torque applied to the body by the CMG is not instantaneous. For this case the torque is not continually applied about the $\hat{b}_3$ axis due to the changing attitude of the body. We see this effect in the attitude error. The momentum wheels cancel out the off $\hat{b}_3$ axis torques. Increasing the momentum wheel gains allows the CMG to provide torques more optimally about the $\hat{b}_3$ axis. By increasing the momentum wheel gains we use momentum wheel torque that the CMG is supposed to be reducing.

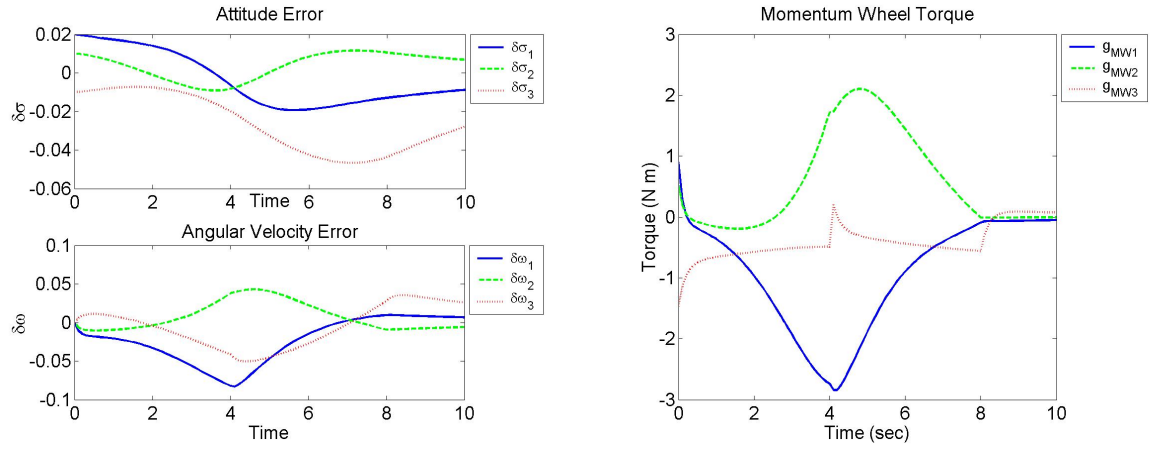

Figure 5.8: *One Open Loop CMG with Lyapunov Momentum Wheel Feedback*

5.5 Control Strategy II Results

The second control strategy attempts to add versatility to the solution of the problem. Preprocessing time, and in turn execution time, can be improved upon from the mixed open and closed loop control strategies. For Control Strategy II there is no preprocessing of a closed-loop CMG law to find the open-loop control. The simulations generate the CMG and momentum wheel control torque together. The exception is the CMG feedback and momentum wheel feedforward control law. For the purposes of simulation, the gimbal rate steering law is again implemented with the state errors. At every time step we use an Euler integration to find the predicted state errors given the CMG control that will be implemented. The Lyapunov control law of Section 4.5.1 is implemented with the predicted errors to provide a feedforward momentum wheel control law.

5.5.1 Parallel CMG/Momentum Wheel Control

Results of numerical simulations of the Control Strategy II are presented. Figure 5.9 show the errors and momentum wheel control torques for the parallel controller. The momentum wheel control effort overshot more than the controllers of Section 5.4. The overshoot can be attributed to the combination of the two control laws over-compensating for the error. Despite the large control effort, the system still converges to the reference trajectory.

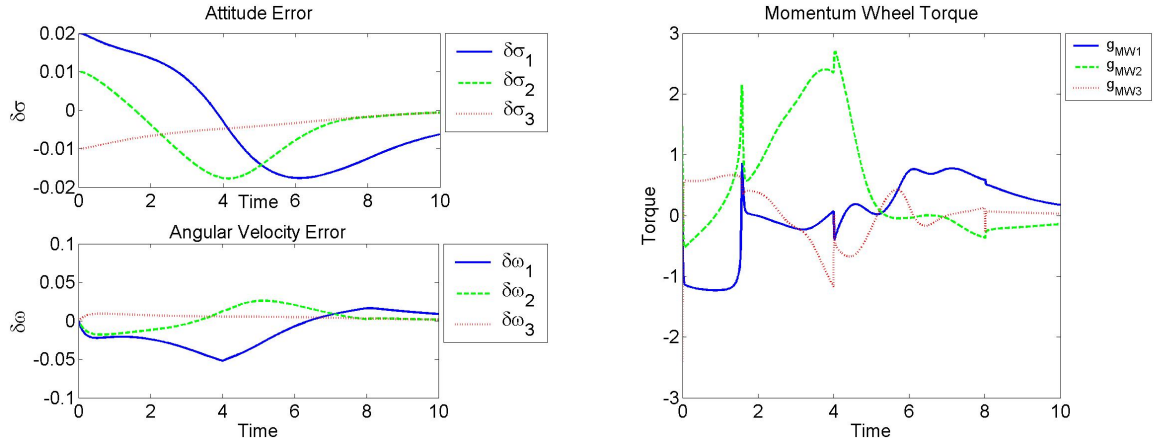

Figure 5.9: *Parallel CMG/Momentum Wheel Control*

5.5.2 Parallel CMG/Independant Momentum Wheel Control

The parallel CMG and independent momentum wheel controller attempts to compensate for the overshoot of the parallel controller by withholding CMG knowledge from the momentum wheel control law. We use the momentum wheel Lyapunov controller of Section 4.5.1 and the CMG controller of Section 4.4 with singularity avoidance of Section 4.4.1. Figure 5.10 shows the parallel CMG/independent momentum wheel control results. The convergence rate is greatly improved by this method and the momentum wheel control torques are decreased versus the parallel CMG/momentum wheel controller. The momentum wheel control effort is reduced by withholding knowledge of the CMGs from the controller.

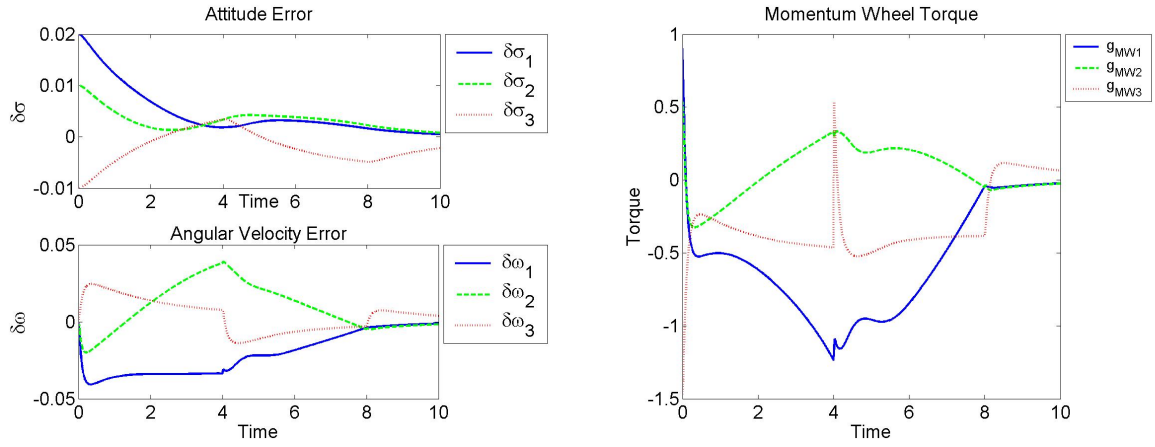

Figure 5.10: *Parallel CMG/Independent Momentum Wheel Control*

5.5.3 CMG Feedback with Momentum Wheel Feedforward Control

A momentum wheel feedforward control is implemented with the CMG gimbal rate control law. Numerical results of CMG closed loop and momentum wheel feedforward are shown in Figure 5.11. The momentum wheel control effort is similar in magnitude to the previous controller; however the torque profile shows appreciable differences. The convergence of tracking error is similar to that of the parallel CMG and independent momentum wheel controller in Figure 5.10.

The developed controllers have been numerically simulated. In the next section we examine selected controllers for differing slew rates with and without initial condition errors.

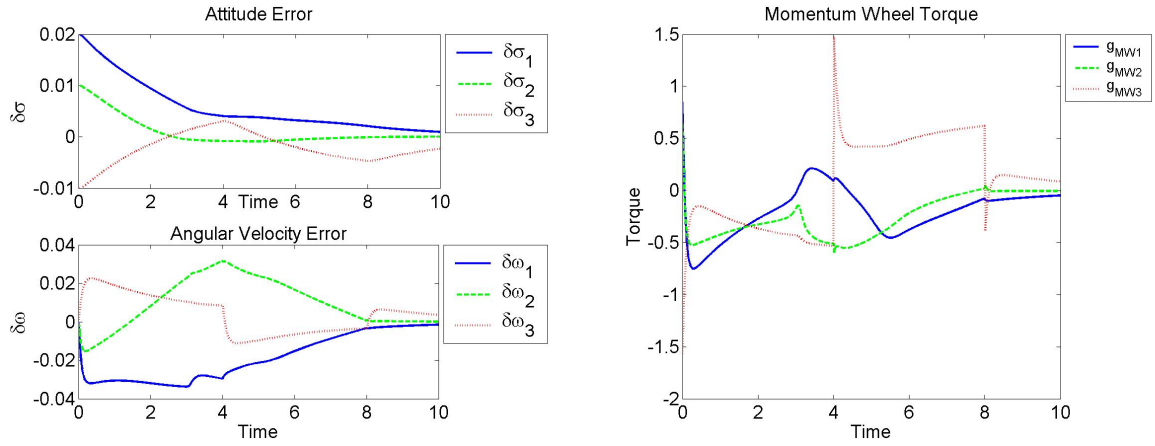

Figure 5.11: *CMG Feedback with Momentum Wheel Feedforward Control*

5.6 Trend Analysis

We explore the usefulness of these control strategies for differing reference reorientation rates. We use the same reference motion of the prior section with exception to the reorientation rate. The reference motion is a 90° slew about the $\hat{b}_3$ axis. The external torque applied to the reference body is varied in magnitude in order to vary the time of reorientation and angular velocities. Bang-bang control is used with the external torques listed in Table 5.3. The 'Time' is the acceleration time for the reference body. The initial conditions of the spacecraft remain $\delta\boldsymbol{\sigma} = [0.02, 0.01, -0.01]^T$ and $\delta\boldsymbol{\omega} = [0, 0, 0]^T$.

Table 5.3: Reference Torque Magnitude and Duration

Time (s)	Reference Torque (Nm)
17.72	0.05
12.53	0.10
7.93	0.25
5.60	0.50
4.58	0.75
3.96	1.00
3.54	1.25
3.24	1.50
2.20	3.25
1.77	5.00
1.45	7.50
1.25	10.00
1.12	12.50
1.02	15.00

We square the control torques for each actuator and integrate over the maneuver time to illustrate the magnitude of the CMG gimbal axis torque and the momentum wheel torque for the differing slew rates. Each point can be thought of as the amount of total effort required for a maneuver about a given control axis squared. This control effort measure has units of $(\text{Nm})^2\text{sec}$. Throughout this section we evaluate the following four controllers: CMG open loop with Lyapunov momentum wheel feedback, CMG open loop with momentum wheel feedback linearization, parallel CMG/Lyapunov momentum wheel feedback, and CMG feedback with momentum wheel feedforward control.

Figure 5.12 shows the control effort quantity for the gimbal axes and the momentum wheels for the CMG open loop and Lyapunov feedback momentum wheel control law of Section 4.5.1. The open loop CMG control is found with the controller of Section 4.4 with the singularity avoidance of Section 4.4.1. The control effort for all actuators generally exponentially decreases with reorientation rate. The singularity avoidance produces more control effort for certain reorientation rates where singularities are avoided. Thus making the control effort non-monotonically decreasing with reorientation rate. The control effort for the momentum wheels is more than an order of magnitude greater than that of the CMGs, which demonstrates the torque advantage of CMGs over momentum wheels.

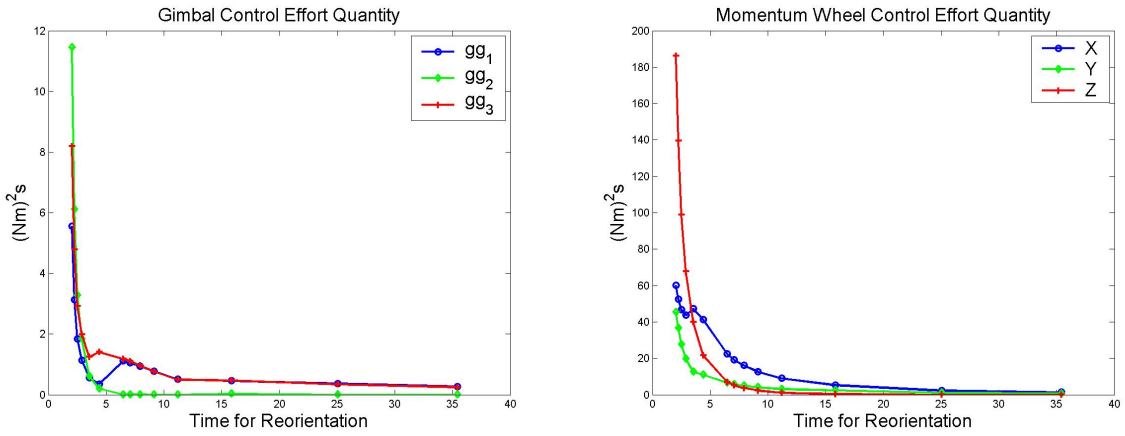

Figure 5.12: *Control Effort Quantity for CMG Open Loop with Lyapunov Momentum Wheel Feedback Control*

Figure 5.13 shows the control effort quantities for the gimbal axes and momentum wheels for the CMG open loop and momentum wheel feedback linearization controller. Note that the gimbal control effort is identical to that of Figure 5.12. We expect the gimbal effort to be the same since the CMG maneuvers are identical for both controllers. The singularity avoidance is utilized with reorientation times from 2 to 5 seconds. The singularity avoidance effects on tracking can be seen in the increase in momentum wheel control effort. The momentum wheel control effort generally decreases with reorientation rate with the exception being the 'X' axis torques.

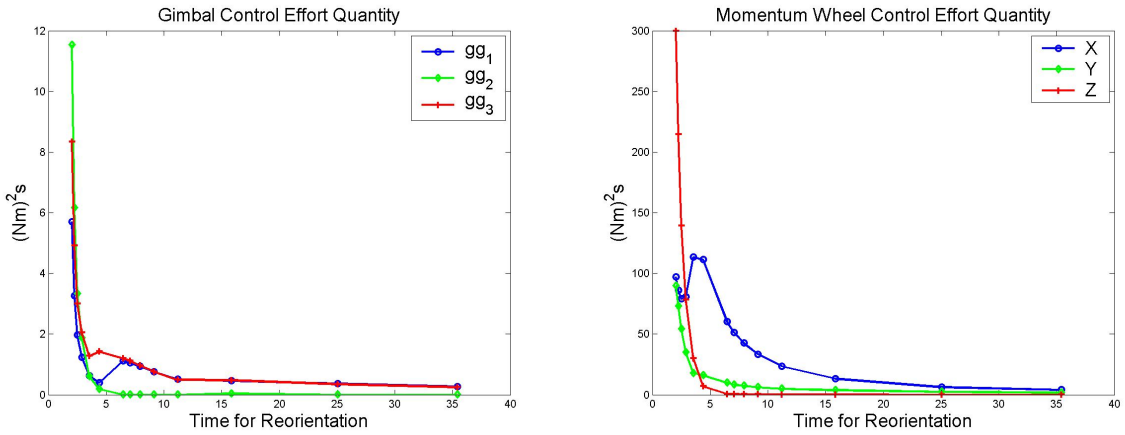

Figure 5.13: *Control Effort Quantity for CMG Open Loop Control with Momentum Wheel Feedback Linearization*

The control effort quantities for the gimbal axes and the momentum wheels are shown in Figure 5.14 for the parallel controller. The control effort for the CMGs is approximately double that of the open loop CMG controller. The actuators over compensate due to each other which is evident in the increase in gimbal control effort. The momentum wheel control effort monotonically decreases with reorientation rate.

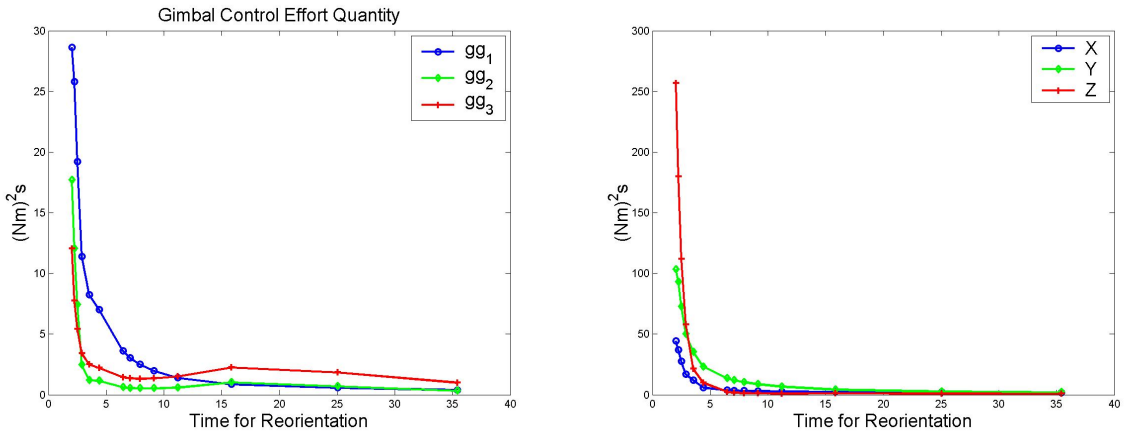

Figure 5.14: *Control Effort Quantity for Parallel CMG/Momentum Wheel Control*

Figure 5.15 is the control effort quantities for the CMG closed loop and momentum wheel feedforward control law. For this controller the CMG control effort is generally greater than the open loop CMG controller. However the momentum wheel control effort is much less with all reorientation rates versus the Strategy I controllers. The 'X' & 'Y' axis torques are an order of magnitude smaller for the CMG closed loop and momentum wheel feedforward controller.

Numerical simulations have been performed for many slew rates with several controllers with initial condition errors. To illustrate the effectiveness of the control laws we simulate the control effort for the same slew rates and controllers without initial condition errors. The parallel results to Figures 5.12 - 5.15 are in Appendix A. We plot the maximum torque required for a reorientation for each controller to evaluate its effectiveness at tracking with minimal momentum wheel control effort. Saturation limits are not considered. Note that in all legends the * superscript denotes a reorientation without initial errors.

Maximum torques for the previously defined cases with initial attitude error and without initial errors are shown. Figures 5.16, 5.17 are the maximum torques for the CMG open loop with Lyapunov and feedback linearization momentum wheel feedback, respectively. Clearly the maximum gimbal torques are the same for both figures and for the cases with and without initial error; the equality is a good "sanity check" since the control

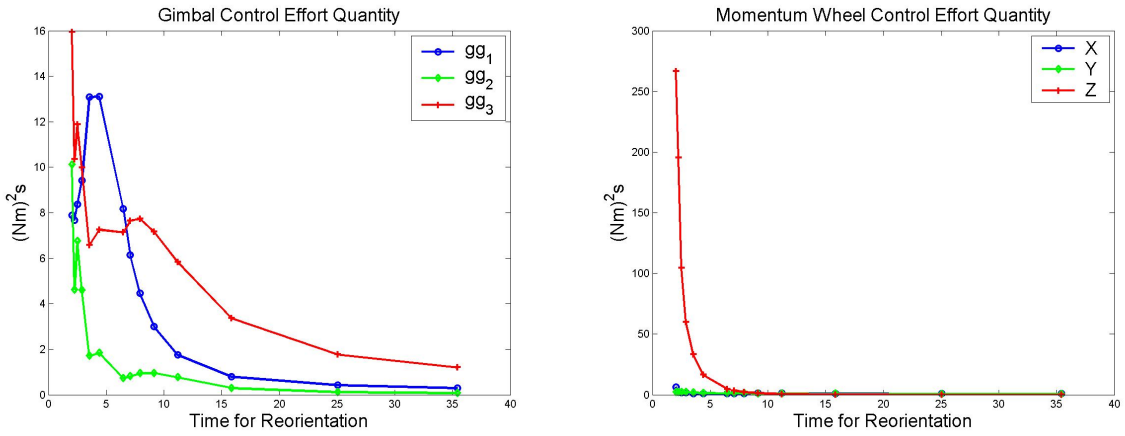

Figure 5.15: *Control Effort Quantity for CMG Feedback Control with Momentum Wheel Feedforward Control*

torques are identical for all cases. The maximum momentum wheel torques decrease

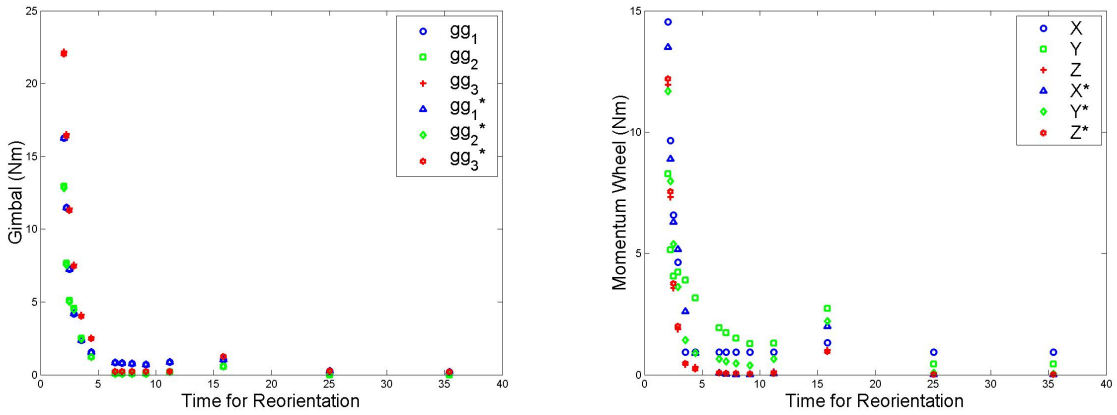

Figure 5.16: *Maximum Control Torques for CMG Open Loop with Lyapunov Momentum Wheel Feedback Control*

with reorientation rate. It also decreases without initial attitude errors as expected. The torque decreases exponentially with reorientation rate.

The controllers with CMG feedback with Lyapunov feedback and feedforward control are shown in Figures 5.18 and 5.19, respectively. Note that the gimbal torques with and without initial errors are different for these controllers. The parallel feedback controller has the greatest maximum torques, which is indicative of the actuators overcompensating

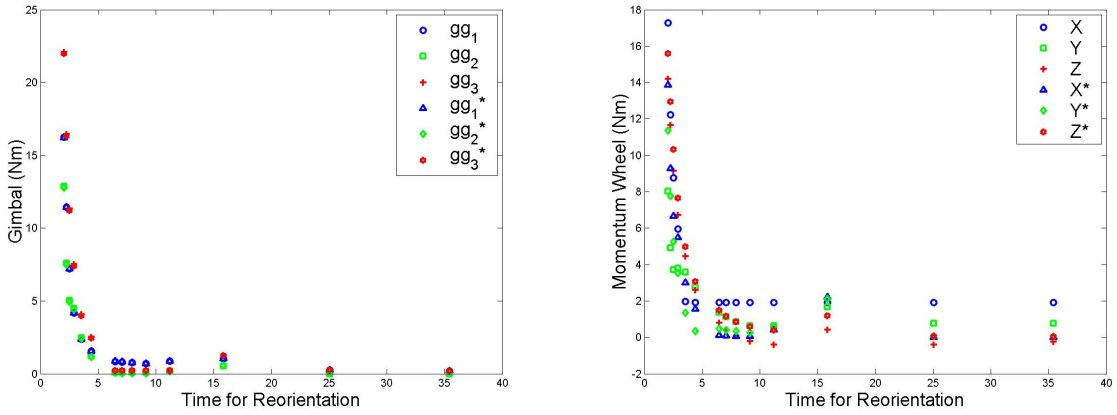

Figure 5.17: *Maximum Control Torques for CMG Open Loop Control with Momentum Wheel Feedback Linearization*

for the tracking errors. The momentum wheel torques for the CMG feedback and mo-

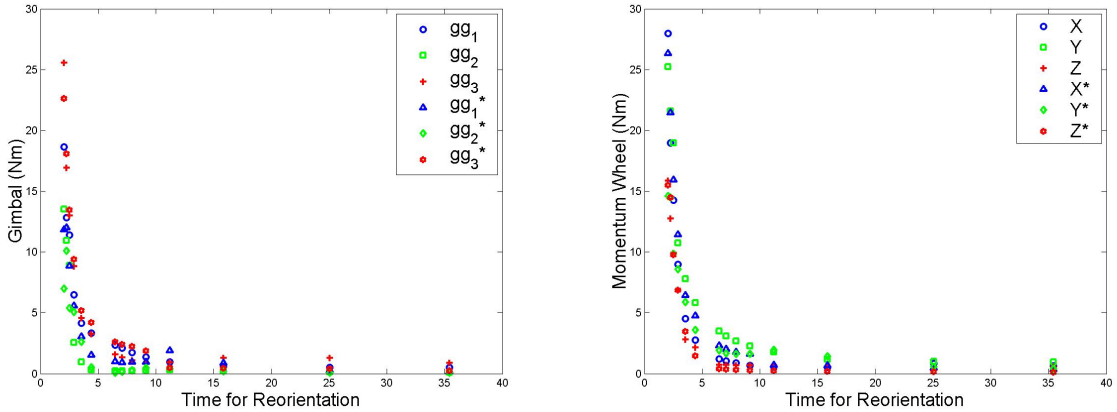

Figure 5.18: *Maximum Control Torques for Parallel CMG/Momentum Wheel Control*

mentum wheel feedforward controller show signs of cooperation between the actuators by generally having lower maximum torques than the other controllers. For the cases with initial errors the momentum wheels adjust for the error and gimbal acceleration torques about the non-reorientation axes. The momentum wheel aligned with the reorientation axis adds torque for reference tracking which causes the CMGs to perform differently than in the previous cases.

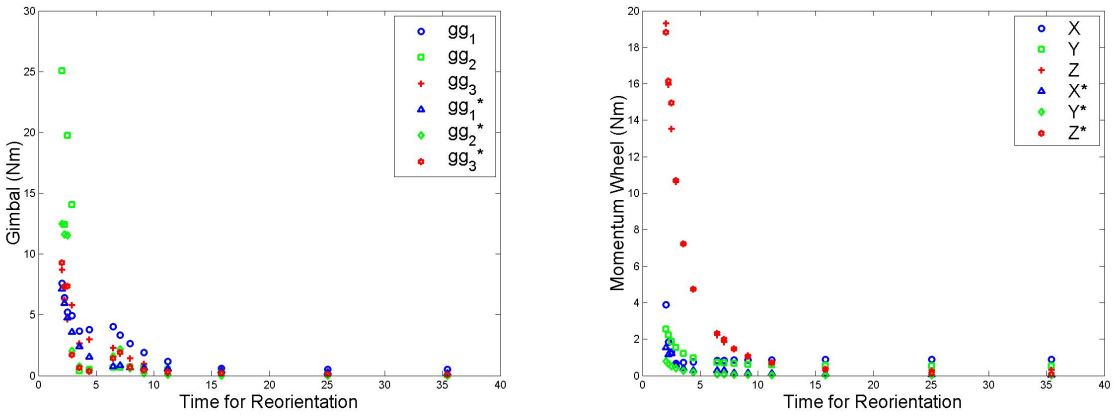

Figure 5.19: *Maximum Control Torques for CMG Feedback Control with Momentum Wheel Feedforward Control*

Chapter 6

Virginia Tech Spacecraft Simulator

In this chapter we describe the spacecraft simulator at Virginia Tech, along with the design of the single gimbal control moment gyro that is integrated on the simulator. Sizing criteria for the CMG is discussed. The mixed actuator attitude control concept is implemented with a single CMG and three momentum wheels. Results from simulator testing are presented. The results verify the effectiveness of mixed actuator attitude control. Sources of errors are presented.

6.1 Whorl-I

The ideal spherical air-bearing testbed would allow its payload unconstrained angular motion in three axes. Actually providing this rotational freedom is difficult and in practice requires constraining payload volume. "Tabletop" style platforms, illustrated in Figure 6.1, provide full freedom of spin in the yaw axis but pitch and roll motion are typically constrained to angles of much less than $\pm 90^\circ$. The main structural deck of a tabletop mounts to the flat face of a hemispherical bearing and components are attached to this structure. Note that the yaw axis is defined to be nominally parallel to the gravity vector.

The Virginia Tech Distributed Spacecraft Attitude Control System Simulator consists of two air bearings from Space Electronics, Incorporated. Each can support a payload of up to 300 lb. The tabletop platform provides full freedom in yaw and $\pm 5^\circ$ of tilt in pitch and roll. As shown in Figure 6.1, the tabletop system, dubbed "Whorl-I", is complete. The primary structure is a 3 ft octagonal aluminum honeycomb plate. Large components are mounted directly to threaded inserts installed in the honeycomb, and

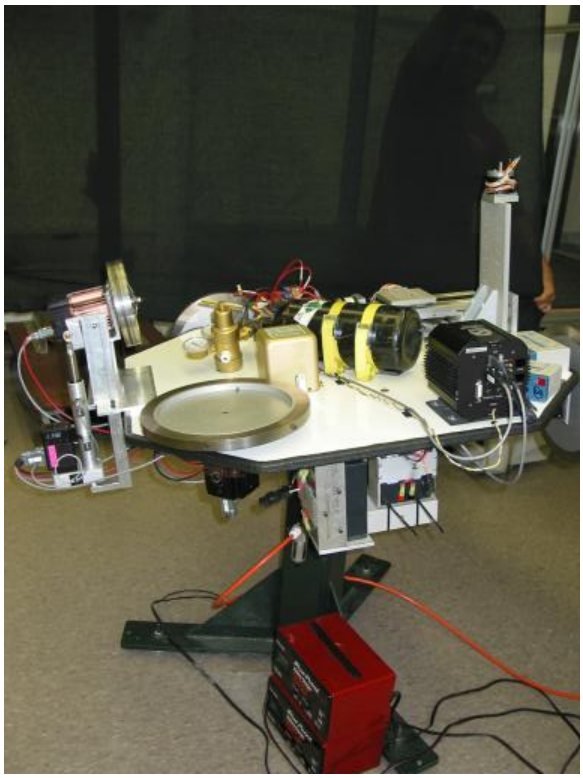

Figure 6.1: *Virginia Tech's Tabletop Spacecraft Attitude Control System Simulator*

smaller components are clustered onto brackets.

Each air bearing is equipped with three-axis accelerometers and rate gyros for attitude determination. The sensors can sense rates up to $\pm 75^\circ/s$ and accelerations up to ± 1.5 g in each axis.

A suite of three custom aluminum/steel 0.075 kg·m^2 wheels mounted on SM3430 Smart Motors can be used as either momentum or reaction wheel devices with a maximum angular momentum of 10 N·m·s and a maximum torque output of 1 N·m. Another SM3430 can be outfitted with a smaller wheel and slewed through a $\pm 45^\circ$ range of angles as a control moment gyro (CMG). Current hardware only supports a single-CMG configuration with a maximum angular momentum of 1.75 N·m·s and a maximum torque of 2 N·m; four-axis CMG control is under consideration.

An important design consideration for air-bearing testbed is collocation of the center-of-rotation of the bearing with the center-of-mass of the system. If the center-of-mass and the center-of-rotation are not coincident the attitude equations of motion of the simulator differ from those of an orbiting satellite: the satellite is free to rotate about its center-of-mass whereas the simulator is constrained to rotate about its center-of-rotation thus an

additional external torque must be modelled. However, modelling the mass distribution of the payload to a sufficiently high resolution is prohibitively complex (*e.g.* including connectors, wiring, or non-uniform density commercial components). We use three orthogonal linear actuators to align the center-of-mass with the center-of-rotation.[3]

6.2 CMG Design

The design of the CMG for implementation on the tabletop spacecraft simulator at Virginia Tech begins with the sizing of the maximum output torque desired from the CMG to the simulator. The CMG is single gimballed for simplicity of hardware and control design. This section covers the method for finding the maximum output torque of the CMG. A discussion of the limitations and concerns in the mechanical design is included. We conclude the section with discussion of the specific hardware used in the CMG.

To size the CMG we first consider that the output torque produced is the change in its angular momentum over time. The frame of the CMG is considered massless for the initial sizing. Figure 6.2(a) depicts a flywheel and the angular momentum vector associated with

Figure 6.2: *Change in Angular Momentum from Gimballing*

the flywheel's inertia and angular velocity about the spin axis. Figure 6.2(b) shows a rotation of the spin axis about a perpendicular axis, the gimbal axis for a CMG. The CMG produces torques about the original spin and transverse axes of $I_{sw}\Omega\cos\delta/\Delta t$ and $I_{sw}\Omega\sin\delta/\Delta t$, respectively. The torque about the transverse axis is the desired output torque. The three variables from the output torque equation that are considered for this design are: the spin axis inertia of the flywheel, flywheel angular speed which is constrained by the spin motor, and the gimbal rate which is constrained by the gimbal motor. Table 6.2 shows the effect of varying the gimbal rate on the output torque generated by the CMG. The nominal spin of the flywheel is 1800 rpm. The gimbal displacement is 45°. For a flywheel spin axis inertia of $I_{sw} = 0.075$ kg m^2 and a nominal spin angular velocity of 2000 rpm, the time required to complete the gimbal displacement is varied. The gimbal rate has a significant impact on the output torque as shown. We use

Table 6.1: Output Torque with Varying Gimbal Rates

Gimbal Time (s)	Output Torque (Nm)
0.50	3.01
0.75	2.01
1.00	1.50
1.25	1.20
1.50	1.00
1.75	0.86
2.00	0.75

a four-bar linkage for gimbal actuation for increased gimbal angle precision as opposed to mounting the flywheel and spin motor directly onto a gimbal motor. A gimbal maneuver with the gimbal motor directly coupled to the flywheel and spin motor only allows for precision up to the level of the encoder in the gimbal motor. A four-bar linkage allows us to choose the ratio between the gimbal angle to motor position. There is also an advantage in torque capability by using the four bar linkage with the same rational.

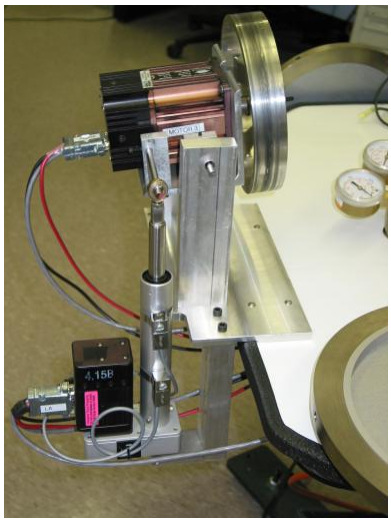

Figure 6.3: *CMG Implemented on Virginia Tech Spacecraft Simulator*

Figure 6.3 shows the constructed CMG. The flywheel is a steel ring with outer diameter of 7.5 inches. The radial thickness of the hub is 0.3 inches. The flywheel is mounted to an

Animatics Smart Motor SM3430 which can spin up to 1800 rpm with the nominal 24 VDC bus of the simulator. The gimbal actuator is an Ultramotion Smart Bug linear actuator, which uses an Animatics Smart Motor SM1720 with an acme nut, 0.2500 inch/rev lead screw. The flywheel and spin motor mount can pivot about an axis perpendicular to the spin axis on two 1/4" diameter Thompson shafts that rotate in bronze bushings. The nose clevis of the linear actuator is attached to the back of the flywheel and spin motor mount. The linear actuator provides $1^\circ/0.01$ inch of stroke or 10°/rev of the lead screw.

The spacecraft simulator design and apparatus have been discussed. We present the results of mixed CMG and momentum wheel attitude control for the simulator in the following section.

6.3 Test Results on Spacecraft Simulator

In this section we present the results of a test run on the spacecraft simulator. Errors caused by the observer are addressed. We present cases of reference tracking with CMG only and momentum wheel only to set a baseline for the mixed control strategies. The mixed CMG and momentum wheel results conclude the section.

The reference motion for the spacecraft simulator is similar to the reference motion used for the numerical simulation of section 5.1. The time for the 90^o slew about the $\hat{b}_3$ axis of $\mathcal{F}_R$ is 17.72 seconds.

The simulator begins tracking with near zero initial condition errors. Small errors are introduced through measurement error and by the table not initially being completely at rest. The flywheel of the CMG has a nominal spin of 2000 rpm. The momentum wheels have a nominal spin about their spin axes of 0 rpm. The results presented in this section are averaged from multiple simulator test runs. The attitude and angular velocity are the observer results and not the actual measured values.

There is a known error in the results. The attitude and angular velocity show errors from the observer. For the system we have no inertial attitude measurement. The observer integrates the measured angular velocities to estimate the current attitude. Integration of the rates propagates noise and drift from the measured rates into the estimated attitude. The uncertainty of the observed states, attitude and angular velocity, propagate into the controller resulting in control torques that do not drive the states to the desired trajectory.

For a baseline we perform the slew maneuver with only the CMG. Figure 6.4 shows the angular velocity and attitude of the spacecraft simulator with respect to the pedestal

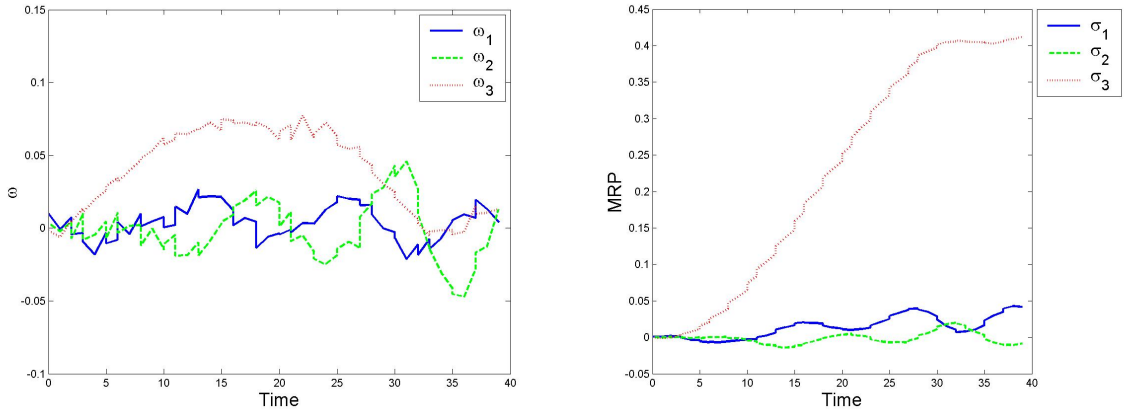

Figure 6.4: *Simulator Angular Velocity and Attitude with CMG Actuation Only*

which we assume to be inertial. The 90^o slew is completed with only the CMG. Disturbance torques from the CMG cause errors about the $\hat{b}_1$ and $\hat{b}_2$ axes.

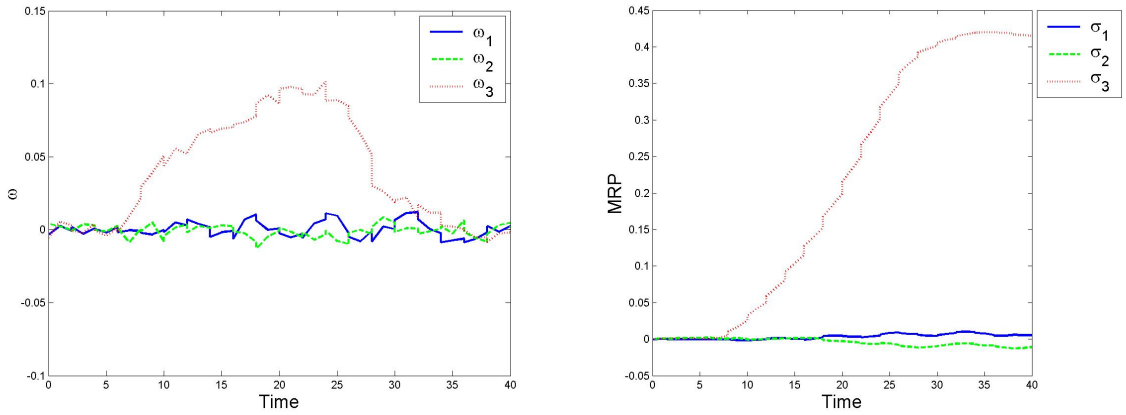

Figure 6.5: *Simulator Angular Velocity and Attitude with Momentum Wheel Actuation Only*

Figure 6.5 shows the angular velocity and attitude of the spacecraft simulator with momentum wheel actuation only. The final attitude is within the uncertainty of the observer. The tracking about the $\hat{b}_1$ and $\hat{b}_2$ axes is also in the the uncertainty range of the observer. The $\hat{b}_3$ axis tracking initially lags behind the reference motion. The lag is caused by the large inertia of the momentum wheels. The commanded torque must be great enough to overcome the static friction and inertia of the flywheel.

The commanded torques from the controller are plotted in Figure 6.6. The $\hat{b}_1$ and $\hat{b}_2$

axis control torques remain in the uncertainty region of the observer. The commanded torques for $\hat{b}_3$ exceed 0.1 Nm. We use the CMG to reduce the momentum wheel torque required about the $\hat{b}_3$ axis.

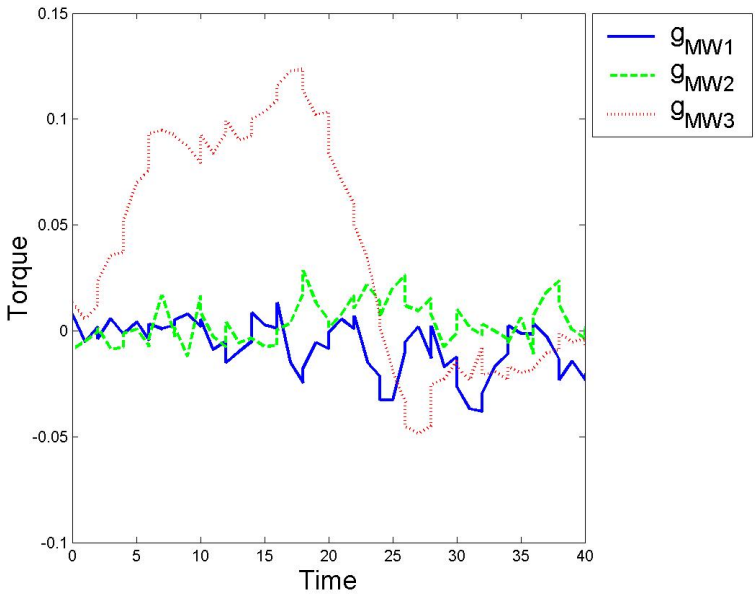

Figure 6.6: *Simulator Momentum Wheel Control Torques with Momentum Wheel Actuation Only*

Remember that the concept of mixed actuator attitude control is to use CMGs to provide large torques for slewing and precision torques for tracking error rejection. Figure 6.7 illustrates the attitude and angular velocity results for the simulator using a CMG and three momentum wheels for actuation. The CMG executes the same maneuver that produced the results of Figure 6.4. The momentum wheels attempt to correct for the tracking errors. Figure 6.8 is the control torques that were commanded to the momentum wheels. The controller provides torque about the slew axis to provide closer tracking to the reference motion than the CMG independently provides. Note that the slew axis momentum wheel do not spin up during the multiple runs of this simulation. The control torques to the momentum wheel did not exceed the torques required to overcome the static friction and the inertia of the flywheel. The off-slew axis control torques attempt to reject the torques created by the CMGs gimballing. The $\hat{b}_1$ and $\hat{b}_2$ momentum wheels generally had non-zero relative angular velocities for the mixed control simulator test runs.

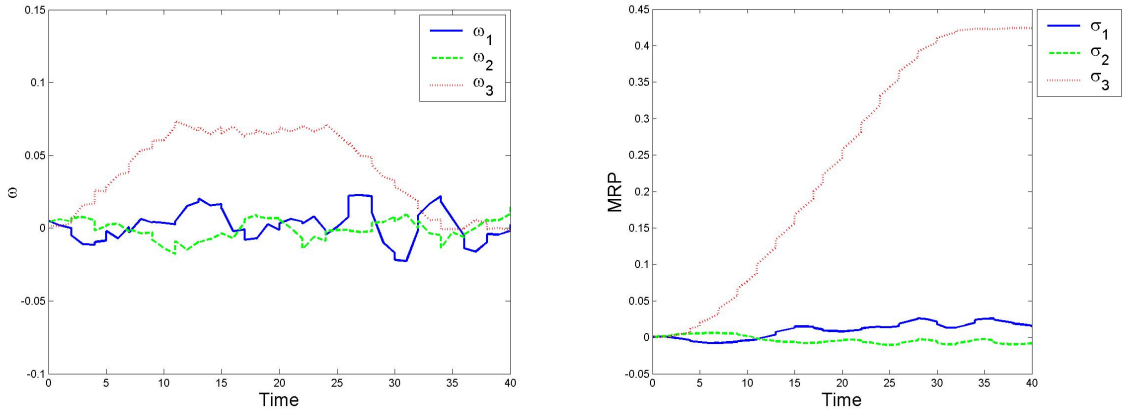

Figure 6.7: *Simulator Angular Velocity and Attitude with Mixed CMG and Momentum Wheel Actuation*

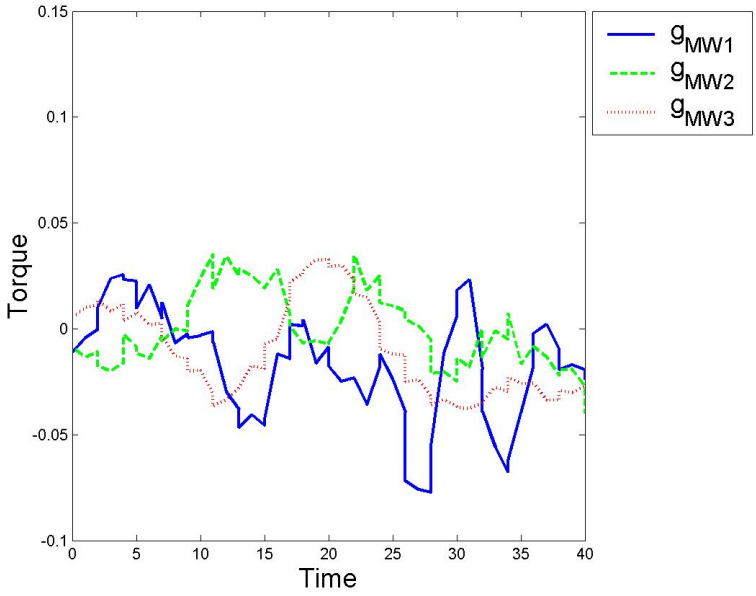

Figure 6.8: *Simulator Momentum Wheel Control Torques with CMG and Momentum Wheel Actuation*

Most importantly, notice the magnitude of the control torques. Compare Figures 6.6 and 6.8 to see the benefit of mixed actuator control. The off-slew control torques are similar in magnitude. The slew axis momentum wheel control torque is approximately half the magnitude for the mixed actuators as compared to the momentum wheel only case.

Chapter 7

Conclusions

Two control strategies are developed for spacecraft attitude control using combinations of control moment gyros and momentum wheels. Numerical simulations and spacecraft simulator testing are used to illustrate mixed actuator attitude control. In this section we review our research and suggest future work.

7.1 Summary

The objective of this research is to derive and validate mixed CMG and momentum wheel control laws. A control moment gyro gimbal rate feedforward control law provides output torques required for large rapid angular slew maneuvers. Lyapunov and feedback linearization techniques are used to develop momentum wheel control laws for initial condition and tracking error rejection. The controllers are derived from the nonlinear state equations for attitude and angular velocity error. Both control laws guarantee asymptotic convergence. Several variations are given based on differing assumptions: $d\mathbf{I}/dt = 0$, no knowledge of the CMGs, reduced number of CMGs. A closed loop multiple actuator controller is presented. A closed loop CMG with momentum wheel feedforward control is presented.

Numerical simulations are performed to verify convergence of the system with the derived control laws. Momentum wheel control torques for each controller are small in comparison to the torques required for the maneuver. Trend analysis for selected controllers shows that generally actuator control effort decreases with reference reorientation rate. Certain CMG configurations and reorientation rates require singularity avoidance, for which the momentum wheel control effort increases. Using *singularity direction avoid-*

ance can reduce the tracking error and momentum wheel control effort that is caused by avoiding CMG singular configurations.

Implementation of one CMG and three orthogonal momentum wheels on a spacecraft simulator illustrated the mixed actuator attitude control concept. The spacecraft simulator had tracking errors due to observer errors. Overall the controller showed promise.

7.2 Recommended Future Work

The focus of this research was to derive mixed CMG and momentum wheel attitude controllers and prove that the derived controllers caused the system to converge to the reference motion. The next step for the derived controllers is optimization of gain selection, and comparison between the controllers with optimal gains. For this purpose the optimal gain solution would minimize control effort. Future work should include power studies of mixed CMG and momentum wheel attitude control versus momentum wheel control to verify the advantage of the mixed actuator attitude control concept.

The configuration of one CMG with a momentum wheel cluster, both in closed loop control, seems promising. The problem is under-constrained, which will require optimal control techniques to solve. Adapting previous null-motion solutions, such as in Ref. [16], to one CMG with momentum wheels might provide a means of optimally configuring the CMG.

Bibliography

[1] B. Wie, Q. Liu, and F. Bauer, "Classical and robust H_∞ control redesign for the Hubble Space Telescope," *Journal of Guidance, Control, and Dynamics*, vol. 16, no. 6, pp. 1069–1077, 1993.

[2] C. D. Hall, P. Tsiotras, and H. Shen, "Tracking rigid body motion using thrusters and momentum wheels," *The Journal of the Astronautical Sciences*, vol. 50, no. 3, 2002.

[3] J. L. Schwartz, M. A. Peck, and C. D. Hall, "Historical review of air-bearing spacecraft simulators," *Journal of Guidance, Control, and Dynamics*, vol. 26, no. 4, pp. 513–522, 2003.

[4] K. A. Ford, *Reorientations of Flexible Spacecraft Using Momentum Exchange Devices*. PhD thesis, Air Force Institute of Technology, Dayton, OH, 1997.

[5] P. Tsiotras, "Stabilization and optimality results for the attitude control problem," *Journal of Guidance, Control, and Dynamics*, vol. 19, pp. 772–779, July 1996.

[6] P. C. Hughes, *Spacecraft Attitude Dynamics*. New York, New York: John Wiley and Sons, 1986.

[7] C. D. Hall, "Spinup dynamics of gyrostats," *Journal of Guidance, Control, and Dynamics*, vol. 18, no. 5, pp. 1177–1183, 1995.

[8] C. D. Hall, "High speed flywheels for integrated energy storage and attitude control," in *Proceedings of the American Control Conference*, (Albuquerque, NM), pp. 1894–1898, June 1997.

[9] C. D. Hall, P. Tsiotras, and H. Shen, "Satellite attitude control and power tracking with momentum/energy wheels," *Journal of Guidance, Control, and Dynamics*, vol. 24, no. 1, pp. 23–34, 2001.

[10] B. T. Costic, *Energy Management and Attitude Control Strategies using Flywheels*. PhD thesis, Clemson University, 2001.

[11] J. L. Junkins, M. R. Akella, and R. D. Robinett, "Nonlinear adaptive control of spacecraft maneuvers," in *Proceedings of the AIAA Guidance, Navigation, and Control Conference*, no. 97-3480, (New Orleans, LA), August 1997.

[12] H. S. Oh and S. R. Vadali, "Feedback control and steering laws for spacecraft using single gimbal control moment gyros," *Journal of the Astronautical Sciences*, vol. 38, pp. 183–203, April 1991.

[13] S. R. Vadali, H. S. Oh, and S. R. Walker, "Preferred gimbal angles for single gimbal control moment gyros," *Journal of Guidance, Control, and Dynamics*, vol. 13, no. 6, pp. 1090–1095, 1990.

[14] S. R. Vadali and S. Krishnan, "Suboptimal command generation for control moment gyroscopes and feedback control of spacecraft," *Journal of Guidance, Control, and Dynamics*, vol. 18, no. 6, pp. 1350–1354, 1995.

[15] B. R. Hoelscher and S. R. Vadali, "Optimal open-loop and feedback control using single gimbal control moment gyroscopes," *The Journal of the Astronautical Sciences*, vol. 42, pp. 189–206, April 1994.

[16] K. A. Ford and C. D. Hall, "Singular direction avoidance steering for control-moment gyros," *Journal of Guidance, Control, and Dynamics*, vol. 23, pp. 648–656, July 2000.

[17] M. R. Rokui and S. Kalaycioglu, "Control moment gyro (CMG) based spacecraft attitude control using feedback linearization control technique," *Advances in the Astronautical Sciences*, vol. 97, no. 1, pp. 983–997, 1997.

[18] H. Schaub, S. R. Vadali, and J. L. Junkins, "Feedback control law for variable speed control moment gyros," *Journal of the Astronautical Sciences*, vol. 46, pp. 307–328, July 1998.

[19] G. Avanzini and G. de Matteis, "A local optimization technique for attitude motion tracking using control moment gyroscopes," *The Journal of the Astronautical Sciences*, vol. 50, no. 2, pp. 213–229, 2002.

[20] C. J. Heiberg, D. Bailey, and B. Wie, "Precision pointing control of agile spacecraft using single gimbal control moment gyroscopes," in *Proceedings of the AIAA Guidance, Navigation, and Control Conference*, no. 97-3757, (New Orleans, LA), August 1997.

[21] B. Wie, C. J. Heiberg, and D. Bailey, "Rapid multi-target acquisition and pointing control of agile spacecraft," in *Proceedings of the AIAA Guidance, Navigation, and Control Conference and Exhibit*, no. 00-4546, (Denver, CO), August 2000.

[22] S. N. Singh and T. C. Bossart, "Exact feedback linearization and control of space station using CMG," *IEEE Transactions on Automatic Control*, vol. 38, pp. 184–187, January 1993.

[23] M. R. Long, "Spacecraft attitude tracking control," Master's thesis, Virginia Tech, Blacksburg, VA, 1999.

[24] M. Casasco and G. Radice, "Autonomous slew maneuvering and attitude control using the potential function method," in *Proceedings of the AAS/AIAA Astrodynamics Specialists Conference*, no. 03-612, (Big Sky, MT), August 2003.

[25] X. Chen and W. H. Steyn, "Robust combined eigenaxis slew maneuver," in *Proceedings of the AIAA Guidance, Navigation, and Control Conference and Exhibit*, no. 99-4048, (Portland, OR), August 1999.

[26] C. M. Roithmayr, C. D. Karlgaard, R. R. Kumar, H. Seywald, and D. M. Bose, "Dynamics and control of attitude, power, and momentum for a spacecraft using flywheels and control moment gyroscopes," *Langley Technical Report*, no. 212178, 2003.

[27] V. Lappas, W. Steyn, and C. Underwood, "Control moment gyro gimbal angle compensation using magnetic control during external disturbances," in *Proceedings of the AIAA Guidance, Navigation, and Control Conference and Exhibit*, no. 01-4339, (Montreal, Canada), August 2001.

[28] H. Schaub and J. L. Junkins, "CMG singularity avoidance using VSCMG null motion," in *AIAA/AAS Astrodynamics Specialist Conference and Exhibit*, no. 98-4388, (Boston, MA), August 1998.

[29] M. A. Peck, L. Miller, A. Cavender, M. Gonzalez, and T. Hintz, "An airbearing-based testbed for momentum control systems and spacecraft line of sight," in *Proceedings of the 13th AAS/AIAA Space Flight Mechanics Meeting*, no. 03-127, (Ponce, Puerto Rico), February 2003.

[30] J. J. Kalley and H. L. Mork, "Development and air bearing test of a double gimballed momentum wheel attitude control system," in *AIAA Communications Satellite Systems Conference*, (Las Angels, CA), April 1974.

[31] A. Ramos, "Air bearing platform testing of a double-gimballed momentum wheel attitude control system," *COMSAT Technical Review*, vol. 5, pp. 53–72, 1975.

[32] H. Kurokawa, "Constrained steering law of pyramid type CMGs and ground tests," in *Proceedings of the AIAA Guidance, Navigation, and Control Conference*, no. 96-3790, (San Diego, CA), July 1996.

[33] J. E. Colebank, R. D. Jones, G. R. Nagy, R. D. Pollak, and D. R. Mannebach, "Simsat: A satellite simulator and experimental test bed for Air Force research," in *Proceedings of the AIAA Space Technology Conference and Exposition*, (Albuquerque, NM), September 1999.

[34] S. Cho and N. H. McClamroch, "Feedback control of triaxial attitude control testbed actuated by two proof mass devices," in *Proceedings of the 41th IEEE Conference of Decision and Control*, (Las Vegas, NV), December 2002.

[35] B. Kim, E. Velenis, P. Kriengsiri, and P. Tsiotras, "A spacecraft simulator for research and education," in *Proceedings of the AIAA Guidance, Dynamics and Control Conference*, no. 01-367, (Reno, NV), pp. 897–914, 2001.

[36] M. D. Shuster, "A survey of attitude representations," *The Journal of the Astronautical Sciences*, vol. 41, no. 4, pp. 439–518, 1993.

[37] H. K. Khalil, *Nonlinear Systems*. New York, New York: Macmillian, 1992.

[38] S. Sastry, *Nonlinear Systems*. New York, New York: Springer, 1999.

[39] J. J. Slotine and W. Li, *Applied Nonlinear Control*. Englewood Cliffs, New Jersy: Prentice Hall, 1991.

[40] H. Schaub and J. L. Junkins, "Matlab toolbox for rigid body kinematics," *Advances in the Astronautical Sciences*, vol. 102, pp. 549–560, 1999.

Appendix A

Trend Analysis Results without Initial Errors

Figure A.1 shows the control effort quantities for the CMG open loop and Lyapunov momentum wheel controller. The control effort for the gimbal axes are the same, as expected, for the simulations with and without initial errors since the CMG maneuver is identical for both. The momentum wheel effort is less without initial errors, which shows that the momentum wheels are correcting for the errors from the gimbal acceleration and inertias only.

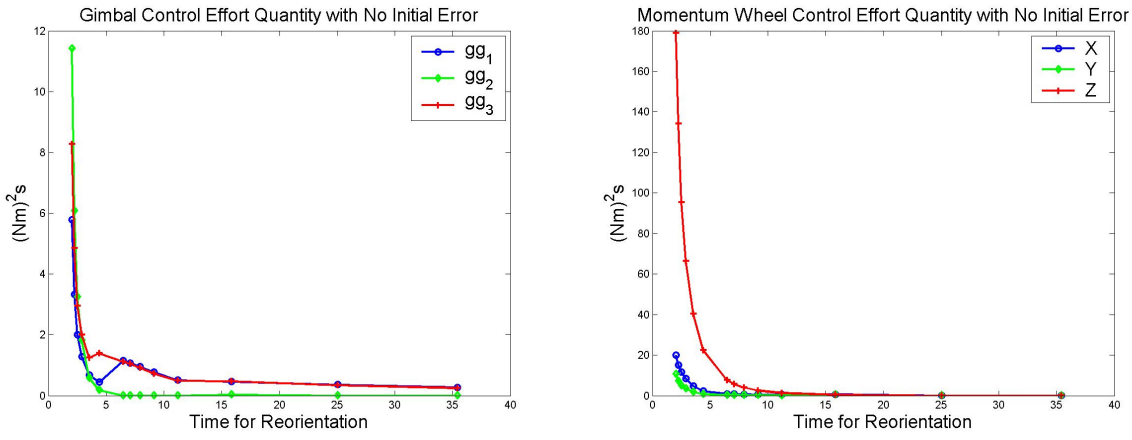

Figure A.1: *Control Effort Quantity for CMG Open Loop with Lyapunov Momentum Wheel Feedback Control without Initial Errors*

Figure A.2 is the control effort quantities for CMG open loop and feedback linearization

using momentum wheels. The CMG control effort is the same as the case with errors as previously discussed. The momentum wheel control efforts about the 'X' and 'Y' axes are much less than the cases with initial errors. The 'Z' axis control effort is large for reorientations of 5 seconds or less, and almost null for slower reorientations. The large control effort is caused by singularity avoidance.

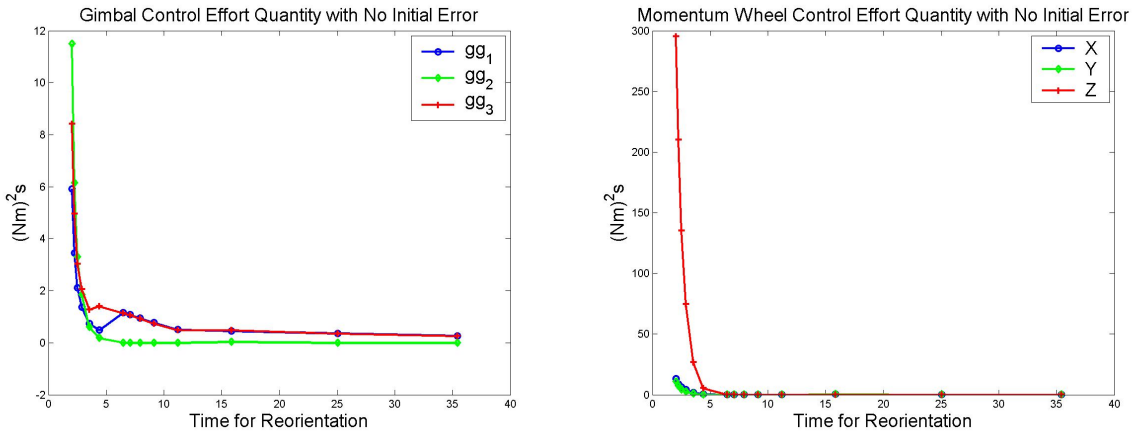

Figure A.2: *Control Effort Quantity for CMG Open Loop Control with Momentum Wheel Feedback Linearization without Initial Errors*

The control effort quantities for the parallel controller are shown in Figure A.3. The gimbal effort is about half of the case with initial errors. The momentum wheel control effort decreases slightly without initial errors. The decrease in gimbal control effort shows that the CMGs are compensating for the tracking errors, which is not our desired control methodology.

Figure A.4 shows the control effort quantity for the CMG closed loop and momentum wheel feedforward control law. The gimbal and momentum wheel control effort is generally less without initial errors for this controller. The concern is in the small of reorientation control effort for the momentum wheels. As previously discussed, we want the momentum wheels to compensate for tracking errors, not the CMGs.

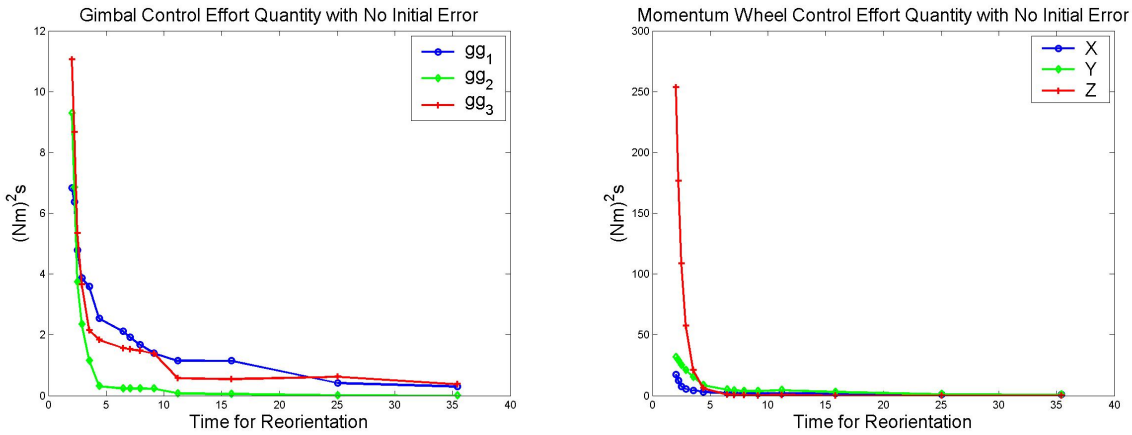

Figure A.3: *Control Effort Quantity for Parallel CMG/Momentum Wheel Control without Initial Errors*

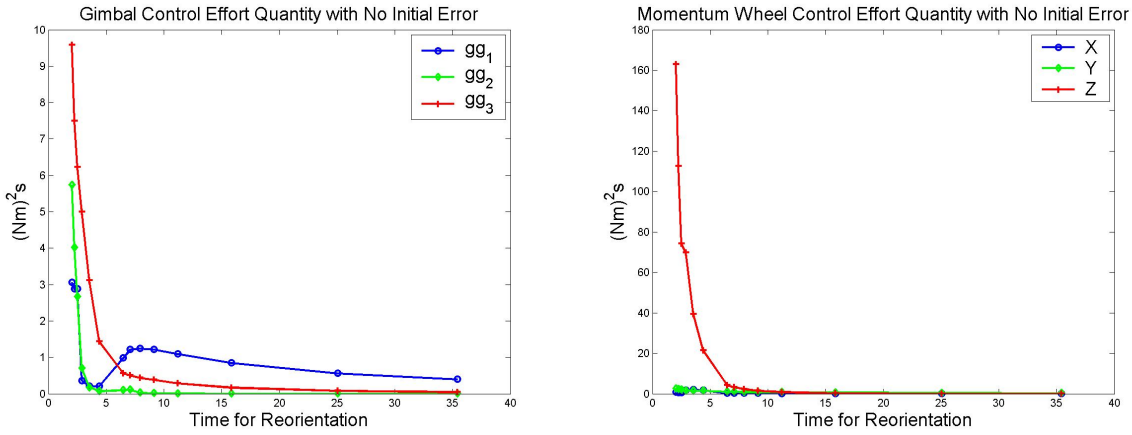

Figure A.4: *Control Effort Quantity for CMG Feedback Control with Momentum Wheel Feedforward Control without Initial Errors*

Vita

Claude Eugene Skelton II was born into an United States Air Force family in Okinawa, Japan. He graduated from Westlake High School in 1996. In the fall of the same year he began college at Virginia Polytechnic Institute & State University (Virginia Tech). He funded his undergraduate career through constant employment, most semesters with multiple jobs. Eugene graduated in May 2000 with a Bachelor of Science in Mechanical Engineering. Eugene was employed in June 2000 by the AVX Corporation in Myrtle Beach, SC as a Mechanical Engineer providing automated machine design.

With hopes of pursuing a more challenging career, he went back for graduate school Virginia Tech in Aerospace Engineering. After a short time he found the Space Systems Simulation Laboratory where he conducted his research on mixed actuator attitude control.

In September 2003 Eugene started with CENTRA Technology, Inc. in Arlington, Virginia. He currently is an Aerospace Engineering Systems Engineering and Technical Analysis (SETA) support contractor for Defense Advanced Research Projects Agency (DARPA) program managers.